Improving Thermal Protection of Cryogenic Tank Cars Through Testing, Analysis, and Evaluation of Pressure Relief Valve System Performance

REPORT DOCUMENTATION PAGE

1. REPORT DATE *(DD-MM-YYYY)* 27-09-2023	2. REPORT TYPE Technical Report	3. DATES COVERED *(From - To)* 8/2022-8/2023

4. TITLE AND SUBTITLE **Improving Thermal Protection of Cryogenic Tank Cars Through Testing, Analysis, and Evaluation of Pressure Relief Valve System Performance**	5a. CONTRACT NUMBER 693JJ633C000012
	5b. GRANT NUMBER
	5c. PROGRAM ELEMENT NUMBER

6. AUTHOR(S) Garrett Mattos: ORCID 0000-0003-4682-7110 Keith Friedman ORCID 0000-0002-3133-4113	5d. PROJECT NUMBER
	5e. TASK NUMBER
	5f. WORK UNIT NUMBER

7. PERFORMING ORGANIZATION NAME(S) AND ADDRESS(ES) Friedman Research Corporation 6500 River Place Blvd, Bldg 7, Ste 250 Austin, TX 78730	8. PERFORMING ORGANIZATION REPORT NUMBER

9. SPONSORING/MONITORING AGENCY NAME(S) AND ADDRESS(ES) U.S. Department of Transportation Federal Railroad Administration Office of Railroad Policy and Development Office of Research, Development, and Technology Washington, DC 20590	10. SPONSOR/MONITOR'S ACRONYM(S)
	11. SPONSOR/MONITOR'S REPORT NUMBER(S) DOT/FRA/ORD-24-01

12. DISTRIBUTION/AVAILABILITY STATEMENT
This document is available to the public through the FRA website.

13. SUPPLEMENTARY NOTES
COR: Francisco Gonzalez, III

14. ABSTRACT
The Federal Railroad Administration (FRA) sponsored a research team to conduct high fidelity finite element (FE) modeling to evaluate the effects of post-derailment motion on PRV system damage and the performance of structural countermeasures. The team conducted physical tests to measure the response of a typical PRV under cryogenic liquid flow as well as the thermal properties of an ignited PRV exhaust plume. Researchers then conducted additional FE modeling to apply the experimentally determined PRV exhaust (i.e., jet) fires to an ISO UN-T75 tank and quantify the tank's response in multiple fire-exposed scenarios.

15. SUBJECT TERMS
Cryogenic fluid, dual phase flow, simulation, fire, LNG

16. SECURITY CLASSIFICATION OF:			17. LIMITATION OF ABSTRACT	18. NUMBER OF PAGES	19a. NAME OF RESPONSIBLE PERSON **Francisco González, III**
a. REPORT	**b. ABSTRACT**	**c. THIS PAGE**		69	19b. TELEPHONE NUMBER *(Include area code)* **202-689-4316**

METRIC/ENGLISH CONVERSION FACTORS

ENGLISH TO METRIC

LENGTH (APPROXIMATE)

1 inch (in)	=	2.5 centimeters (cm)
1 foot (ft)	=	30 centimeters (cm)
1 yard (yd)	=	0.9 meter (m)
1 mile (mi)	=	1.6 kilometers (km)

AREA (APPROXIMATE)

1 square inch (sq in, in^2)	=	6.5 square centimeters (cm^2)
1 square foot (sq ft, ft^2)	=	0.09 square meter (m^2)
1 square yard (sq yd, yd^2)	=	0.8 square meter (m^2)
1 square mile (sq mi, mi^2)	=	2.6 square kilometers (km^2)
1 acre = 0.4 hectare (he)	=	4,000 square meters (m^2)

MASS - WEIGHT (APPROXIMATE)

1 ounce (oz)	=	28 grams (gm)
1 pound (lb)	=	0.45 kilogram (kg)
1 short ton = 2,000 pounds (lb)	=	0.9 tonne (t)

VOLUME (APPROXIMATE)

1 teaspoon (tsp)	=	5 milliliters (ml)
1 tablespoon (tbsp)	=	15 milliliters (ml)
1 fluid ounce (fl oz)	=	30 milliliters (ml)
1 cup (c)	=	0.24 liter (l)
1 pint (pt)	=	0.47 liter (l)
1 quart (qt)	=	0.96 liter (l)
1 gallon (gal)	=	3.8 liters (l)
1 cubic foot (cu ft, ft^3)	=	0.03 cubic meter (m^3)
1 cubic yard (cu yd, yd^3)	=	0.76 cubic meter (m^3)

TEMPERATURE (EXACT)

$[(x-32)(5/9)]$ °F = y °C

METRIC TO ENGLISH

LENGTH (APPROXIMATE)

1 millimeter (mm)	=	0.04 inch (in)
1 centimeter (cm)	=	0.4 inch (in)
1 meter (m)	=	3.3 feet (ft)
1 meter (m)	=	1.1 yards (yd)
1 kilometer (km)	=	0.6 mile (mi)

AREA (APPROXIMATE)

1 square centimeter (cm^2)	=	0.16 square inch (sq in, in^2)
1 square meter (m^2)	=	1.2 square yards (sq yd, yd^2)
1 square kilometer (km^2)	=	0.4 square mile (sq mi, mi^2)
10,000 square meters (m^2)	=	1 hectare (ha) = 2.5 acres

MASS - WEIGHT (APPROXIMATE)

1 gram (gm)	=	0.036 ounce (oz)
1 kilogram (kg)	=	2.2 pounds (lb)
1 tonne (t)	=	1,000 kilograms (kg)
	=	1.1 short tons

VOLUME (APPROXIMATE)

1 milliliter (ml)	=	0.03 fluid ounce (fl oz)
1 liter (l)	=	2.1 pints (pt)
1 liter (l)	=	1.06 quarts (qt)
1 liter (l)	=	0.26 gallon (gal)
1 cubic meter (m^3)	=	36 cubic feet (cu ft, ft^3)
1 cubic meter (m^3)	=	1.3 cubic yards (cu yd, yd^3)

TEMPERATURE (EXACT)

$[(9/5) y + 32]$ °C = x °F

QUICK INCH - CENTIMETER LENGTH CONVERSION

Inches: 0 1 2 3 4 5

Centimeters: 0 1 2 3 4 5 6 7 8 9 10 11 12 13
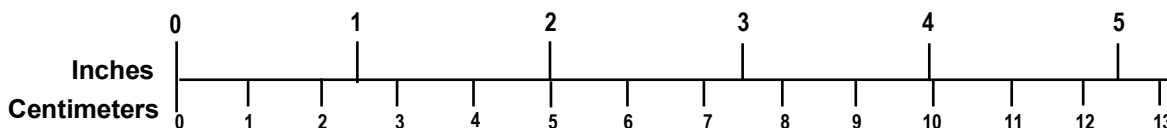
QUICK FAHRENHEIT - CELSIUS TEMPERATURE CONVERSIO

°F	-40°	-22°	-4°	14°	32°	50°	68°	86°	104°	122°	140°	158°	176°	194°	212°
°C	-40°	-30°	-20°	-10°	0°	10°	20°	30°	40°	50°	60°	70°	80°	90°	100°
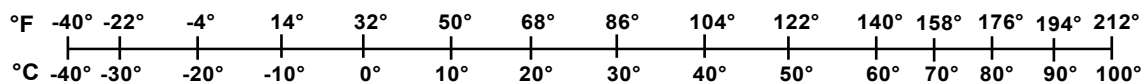
For more exact and or other conversion factors, see NIST Miscellaneous Publication 286, Units of Weights and Measures. Price $2.50 SD Catalog No. C13 10286

Acknowledgements

Contents

Illustrations

Tables

Executive Summary

In a train derailment, tank cars have a high probability of full or partial inversion of tanks and cars. An inversion of a cryogenic tank, such as an ISO UN-T75portable tank, allows liquid or dual-phase fluid to be present at the inlet of the pressure relief valve(s) (PRV). However, PRVs installed on many cryogenic tanks are not specified for use in liquid or dual-phase flow conditions.

The Federal Railroad Administration (FRA) sponsored a research team to conduct high fidelity finite element (FE) modeling to evaluate the effects of post-derailment motion on PRV system damage and the performance of structural countermeasures. The team conducted physical tests to measure the response of a typical PRV under cryogenic liquid flow as well as the thermal properties of an ignited PRV exhaust plume. Researchers then conducted additional FE modeling to apply the experimentally determined PRV exhaust (i.e., jet) fires to an ISO UN-T75 tank and quantify the tank's response in multiple fire-exposed scenarios.

This project builds on previous work, including two full-scale fire tests of ISO UN-T75 tanks filled with cryogenic fluid (i.e., Liquefied Nitrogen and Liquefied Natural Gas) and the development of validated multi-physics models capable of simulating the structural and thermal response of the tank subjected to a pool fire (FRA, 2023).

Key results from the project include:

- A discussion of the derailment mechanisms that are likely to result in the PRV assembly failing to maintain its performance requirements as defined in the regulations

- Identification of crash modes and crash severities that are likely to damage the PRV piping assembly in a way that would decrease its performance

- Characterization of PRV response across a range of tank pressures, ambient conditions, downstream constrictions, and localized heating

- Characterization of low flow rate jet fire thermal response across a range of mass flow rates, orifice sizes, and jet orientations

- Repeatable testing methods

- Demonstration of countermeasures that significantly improve the crashworthiness of the PRV piping assembly

The PRV flow characteristics demonstrated in this project did not negatively affect the fireworthiness of cryogenic tanks in the manner researchers anticipated (i.e., due to degraded flow), but they did present potential challenges related to the effects on neighboring tanks, potentially hindering emergency response, and increasing the rate of content loss. Since the PRV exhaust rates under liquid flow are far greater than under vapor/gas flow, a tank would completely empty its contents within 60 to 125 minutes of PRV activation in a pool fire scenario. While this may reduce the likelihood of a Boiling Liquid Evaporating Vapor Explosion (BLEVE) from occurring, it increases the risk of a vapor cloud and the environmental risk due to content loss. Additionally, the jet fire that would likely be produced from the discharged flammable fluid could impinge on neighboring tanks up to 100 ft away and apply sufficient heating to endanger their contents. Emergency responders need to be aware of the higher

potential for vapor cloud generation due to the greater mass flow rates as well as the danger of cryogenic dual-phase PRV exhaust and substantial jet fire potential.

1. Introduction

The Federal Railroad Administration (FRA) sponsored a research team to conduct high fidelity finite element (FE) modeling to evaluate the effects of post-derailment motion on pressure relief valve (PRV) system damage and the performance of structural countermeasures. The team conducted physical tests to measure the response of a typical PRV under cryogenic liquid flow as well as the thermal properties of an ignited PRV exhaust plume. Researchers then conducted additional FE modeling to apply the experimentally determined PRV exhaust (i.e., jet) fires to an ISO UN-T75 tank and quantify the tank's response in multiple fire-exposed scenarios.

The Pipeline and Hazardous Materials Safety Administration (PHMSA) issued a final ruling on July 24, 2020 (effective on August 24, 2020) that allowed liquefied natural gas (LNG) to be transported by rail in approved tank cars (i.e., enhanced DOT-113 tank cars). In prior research, the team worked for several years with FRA and Transport Canada to conduct physical tests and create computer models of fire-involved UN-T75 portable tanks to quantify their performance and risk of failure. Previous findings related to cryogenic tank response during derailment, tank inversion, and fire exposure prompted this follow-on work to investigate the performance of the PRV system. This report describes the results of physical testing and physics-based numerical modeling used to quantify the performance of the PRV system under derailment conditions and how that performance might lead to potential cascading effects.

1.1 Background

PRVs in cryogenic intermodal tanks and tank cars are necessary to prevent the buildup of interior tank pressure when exposed to fire conditions that can lead to catastrophic failure such as a Boiling Liquid Expanding Vapor Explosion (BLEVE). The likelihood of tank failure under fire conditions is directly related to the ability of the PRV system to perform properly. Crash conditions, final tank position (i.e., rollover angle), and PRV system damage have the potential to alter PRV performance. Preliminary component-level testing conducted by the project team for a Transport Canada project demonstrated that cryogenic fluid flow through PRVs used on UN-T75 tanks (i.e., spring-loaded, PTFE sealed, single-phase flow devices) can significantly reduce performance under certain conditions. In the same project it was shown that the jet flame generated from exhausting high velocity natural gas through the PRV can impinge on a neighboring tank and induce a localized heat flux greater than that generated from a pool fire. The results of FRA's most recent UN-T75 fire test supported this finding (FRA, 2023). An example of a PRV-exhaust jet fire during a fire test of an LNG-filled UN-T75 tank is shown in Figure 1.

Figure 1. Jet Fire of PRV exhaust during fire test of LNG filled UN-T75 tank (FRA, 2023)

In this study, the research team characterized PRV performance under inverted and elevated pressure conditions and related PRV performance to the probability of tank failure under fire conditions. The researchers then present countermeasures to prevent negative outcomes.

1.2 Objectives

The objectives of this project were to:

- Identify PRV performance and design requirements from the regulatory and scientific literature

- Use validated FE models to estimate the damage caused to the PRV system during select derailment scenarios

- Measure PRV performance under cryogenic liquid flow conditions through physical testing

- Conduct physical tests to measure the thermal output of an ignited gas jet

- Quantify the effect of measured PRV performance and jet flame exposure on the risk of tank failure

1.3 Overall Approach

The research team used a combination of multi-physics modeling and physical testing to measure and predict the performance of individual components for a full-scale tank in derailment and fire-exposed conditions. FE modeling of a UN-T75 tank was used to simulate the damage to the PRV piping assembly during derailment scenarios. Eight PRV devices, typical of the style installed on multi-modal cryogenic LNG tanks, were tested under cryogenic liquid flow conditions representative of an inverted tank using liquefied nitrogen (LN2) in place of LNG. PRV tests were conducted at multiple tank pressures, PRV temperatures, downstream constriction levels, environmental conditions, and exhaust pipe lengths. Separate tests were conducted to characterize the heat flux generated by ignited natural gas jets at different flow rates, orientations, and orifice diameters. The data generated from the physical tests were used to inform the inputs of previously validated multi-physics models of fire exposure on a UN-T75 tank. Previous test data and modeling approaches generated through projects with FRA and Transport Canada served as a foundation to this work.

1.4 Scope

This twelve-month project used virtual and physical testing to evaluate the performance of a UN-T75 tank under derailment conditions, PRVs under cryogenic liquid flow conditions, and the resulting effect on tank response when exposed to fire.

1.5 Organization of the Report

The results of a literature and regulation review are presented in Section 2, followed by the results of crashworthiness simulations in Section 3. Physical testing, which relied on the information obtained from the literature review and the simulations, is presented in Section 4 and Section 5. The demonstration of countermeasures through FE analysis and the characterization of tank thermal response to jet fires are provided in Section 6 and Section 7. Suggested future work

4

is discussed in Section 8, and conclusions are presented in Section 9. Fabrication and Test Setup schematics are presented in Appendix A and Appendix B.

2. Literature Review of PRV Characteristics

The research team reviewed selected literature, specification sheets, and American Society of Mechanical Engineers (ASME) regulations to identify the performance ranges, design types, and most commonly used PRVs for cryogenic tanks. Fire exposure to PRVs has been shown to reduce the effective set pressure due to thermal weakening of the internal spring (Prabhakaran et al, 2022), although these tests artificially protected the PRV seals during initial heating. During the fire testing of an ISO UN-T75 tank with LNG (FRA, 2023) the seals on every external valve were observed to fail, leak gas, and produce a flame. The discharge of flammable material through PRVs has been observed to increase the severity of the impinging fire (Prabhakaran et al, 2022). Most manufacturers provide some warning about using gas/vapor-only PRVs in liquid or dual-phase flow conditions (e.g., "Using a standard gas certified trim to flow liquids creates chatter and damages valve components. This is not recommended." (Baker Hughes, n.d.)).

2.1 Key PRV Requirements

The review findings specific to PRV design on multi-modal tanks are summarized below.

- The device type must be spring-loaded[1].
  - Seals for such devices are predominantly Polytetrafluoroethylene (PTFE) with a maximum service temperature of 500°F.
- The device must fully open at 110 percent maximum allowable working pressure (MAWP) and fully close at 10 percent below the discharge pressure[2].
- The valve capacity is determined with the assumption of gas/vapor flow and must be sufficient to prevent the tank from exceeding the test pressure when under complete fire engulfment.
- The discharge capacities for these types of valves typically ranges from 36 to 3162 CFM for set pressures between 10 and 400 psi. (Rockwood Swendeman, n.d.).
  - There were no significant differences noted regarding performance or design of spring-loaded valves between manufacturers.
- PRVs were most commonly situated external to the tank and often within a metal cabinet.

The PRV selected for testing (Rockwood Swendeman 710NEGH-A114; see Section 4 and Section 5) meets all the above criteria for an ISO UN-T75 tank and was used in two full scale fire tests.

Key design features of the PRV piping assembly include:

- Backpressure must be minimized, and obstructions prevented within the PRV piping assembly[3]

---

[1] 49 CFR § 178.274.f.1.v

[2] 49 CFR § 178.277.e.1

[3] 49 CFR § 178.274.f.2

- All PRV inlets must be situated in the vapor space

- Escaping vapor must be directed away from the shell so that it cannot impinge on the shell

Table 1 summarizes the potential consequences of a derailment and correlates them with the performance requirements outlined in the regulations. This study shows that derailment scenarios can result in a tank no longer meeting the design or performance requirement outlined in 49 CFR 178. Specifically, damage during a derailment could constrict flow within the PRV piping assembly (inlet and outlet). A tank inversion would cause the PRV inlet to move from the vapor space into the liquid space. Even without a derailment or tank inversion, the escaping vapor from one tank, ignited or not, could impinge on a neighboring tank shell.

Table 1. Potential effects of a derailment and the associated regulation

Derailment Effect	Secondary Effect	Affected Requirement
Damage to PRD upstream piping	Obstruction leading to PRD which might restrict flow	178.274.f.2
Damage to PRD outlet piping	Increased back-pressure on relieving device	178.274.f.2
	Deformed outlet piping becomes directed toward the tank shell	178.274.f.3.i
None	As-designed PRD outlet may be nominally directed at a neighboring tank	178.274.f.3.i
Rotated or inverted tank	PRD inlet no longer in the vapor space	178.274.f.3.i
Damage to general tank structure	Protect the devices from damage caused by the portable tank overturning	178.274.f.3.ii
Pool fire impingement upon PRD	Damage to seals and/or closing mechanism (i.e., spring) prevents closing at 10% below discharge pressure or fully closing at all	178.277.e.1

2.2 Comprehensive PRV Requirements

A more extensive summary of the regulatory requirement review is provided below.

Performance-Related Requirements of Pressure Relief Devices for UN Portable Tanks[4]

- Types[5]

  - Spring Loaded

  - Frangible Disc (not acceptable for liquified gases)

  - Fusible Elements (not acceptable for liquified gases)

- Rated flow capacity shall be marked on the device [using Standard Cubic Meter Per Second] (SCMS) [6]

---

[4] 49 CFR § 178.274 – Specifications for UN portable tanks

[5] 49 CFR § 178.274.f.1.v

[6] 49 CFR § 178.274.f.1.v

- For Spring-Loaded PRD the rated flow capacity must be determined according to ISO 4126-1 (including Technical Corrigendum 1) and ISO 4126-7 (IBR, see § 171.7 of subchapter)
- Cross sectional flow areas marked on the device (mm^2)

- Connections to PRDs[7]

  - There must be no obstruction in an opening leading to a vent or PRD which might restrict or cut-off the flow from the shell to the device.

  - Vents or pipes from the pressure relief device outlets, when used, must deliver the relieved vapor or liquid to the atmosphere in conditions of minimum backpressure on the relieving devices.

- Location of PRDs[8]

  - All PRD inlets must be situated in the vapor space of the shell.

  - The escaping vapor must be directed away from the shell in such a manner that it cannot impinge upon the shell.

  - Provisions must be implemented to protect the devices from damage caused by the portable tank overturning.

Performance-Related Requirements of Pressure Relief Devices for UN Portable Tanks transporting refrigerated or liquefied gases[9]

- Opening and closing of PRDs[10]

  - Must open automatically at a pressure not less than the MAWP and be fully open at a pressure equal to 110% of the MAWP.

  - Must close at a pressure not lower than 10 percent below the pressure at which discharge starts and must remain closed at all lower pressures.

- Capacity and setting of PRDs[11]

  - In the case of a loss of vacuum or loss of 20 percent of the insulation insulated with solid materials the combined capacity of all PRDs must be sufficient so that the pressure (including accumulation) inside the shell does not exceed 120 percent of the MAWP.

  - Under the circumstances described in paragraphs (e)(4)(i) and (e)(4)(ii) of this section, together with complete fire engulfment, the combined capacity of all

---

[7] 49 CFR § 178.274.f.2

[8] 49 CFR § 178.274.f.3

[9] 49 CFR § 178.277 - Requirements for the design, construction, inspection and testing of portable tanks intended for the transportation of refrigerated liquefied gases.

[10] 49 CFR § 178.277.e.1

[11] 49 CFR § 178.277.e.4

pressure relief devices installed must be sufficient to limit the pressure in the shell to the test pressure.

- o The required capacity of the relief devices must be calculated in accordance with CGA Pamphlet S-1.2 (IBR, see § 171.7 of this subchapter).

Definitions

- Portable Tank[12]: Portable tank means a bulk packaging (except a cylinder having a water capacity of 1000 pounds or less) designed primarily to be loaded onto, or on, or temporarily attached to a transport vehicle or ship and equipped with skids, mountings, or accessories to facilitate handling of the tank by mechanical means. It does not include a cargo tank, tank car, multi-unit tank car tank, or trailer carrying 3AX, 3AAX, or 3T cylinders.

- UN Portable Tank[13]: an intermodal tank having a capacity of more than 450 liters (118.9 gallons). It includes a shell fitted with service equipment and structural equipment, including stabilizing members external to the shell and skids, and mountings or accessories to facilitate mechanical handling. A UN portable tank must be capable of being filled and discharged without the removal of its structural equipment and must be capable of being lifted when full. Cargo tanks, rail tank car tanks, non-metallic tanks, non-specification tanks, bulk bins, and IBCs and packagings made to cylinder specifications are not UN portable tanks.

- MAWP[14]: Maximum allowable working pressure (MAWP) means the maximum effective gauge pressure permissible at the top of the shell of a loaded portable tank in its operating position including the highest effective pressure during filling and discharge.

- Shell[15]: Shell means the part of the portable tank which retains the refrigerated liquefied gas intended for transport, including openings and their closures, but does not include service equipment or external structural equipment.

- Test Pressure[16]: Test pressure means the pressure to which a tank is subjected to determine structural integrity.

---

[12] 49 CFR § 171.8

[13] 49 CFR § 171.8

[14] 49 CFR § 178.277

[15] 49 CFR § 178.320

[16] 49 CFR § 178.320

3. FE Simulation of Crash Conditions

Researchers generated and validated thermal and structural FE models of an ISO UN-T75 tank in previous efforts (Friedman & Mattos, 2018; Mattos & Friedman, 2023). The structural model has been used to simulate rollovers, impacts with fixed objects, and impacts with other railcars and tanks to investigate the risk of internal tank failure and loss of contents. This model has been modified in this project to include pertinent internal and external PRV piping assembly features. The model was then subjected to simulated impacts to determine the threshold impact velocity producing PRV piping assembly damage.

3.1 FE Model Description

The existing FE model of the UN-T75 tank was modified using PRV piping assembly details provided by Taylor Wharton via drawings and images (Figure 2). These were converted to CAD, meshed within LS-DYNA, and added to the existing full model. The materials were defined using temperature-dependent thermal and structural properties based on data from the literature and previously validated material models.
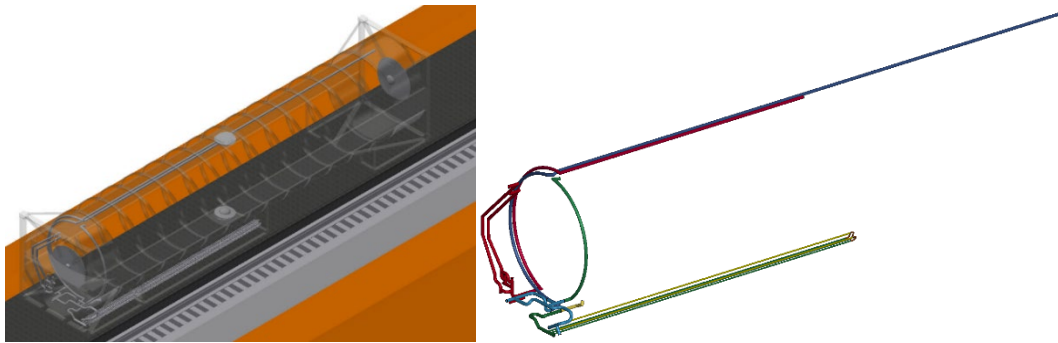
Figure 2. Modified FE model of UN-T75 tank with added PRV piping assembly shown with surrounding environment (left) and with isolated piping assembly (right) [LS-DYNA]

For all simulations, the UN-T75 tank model was placed on top of a flatbed railcar representative of Bethlehem Steel Series car and attached at each corner with constraints representing 150 kN ultimate strength twist-locks as per ISO 1496 (Figure 3). The entire vehicle was placed on standard freight rails on a standard cross section of mainline track (Figure 4). This placed the initial center of gravity of the tank at about 10 feet above the adjacent sub-ballast section. The tank was modeled as full of LNG, which was simulated using smooth particle hydrodynamics (Figure 5). For all simulations the ground and fixed objects (e.g., pole impact) were assumed to be rigid. Other vehicles were modelled with elastic-plastic material properties.

Figure 3. Physical and FE model of UN-T75 tank positioned on flatbed railcar
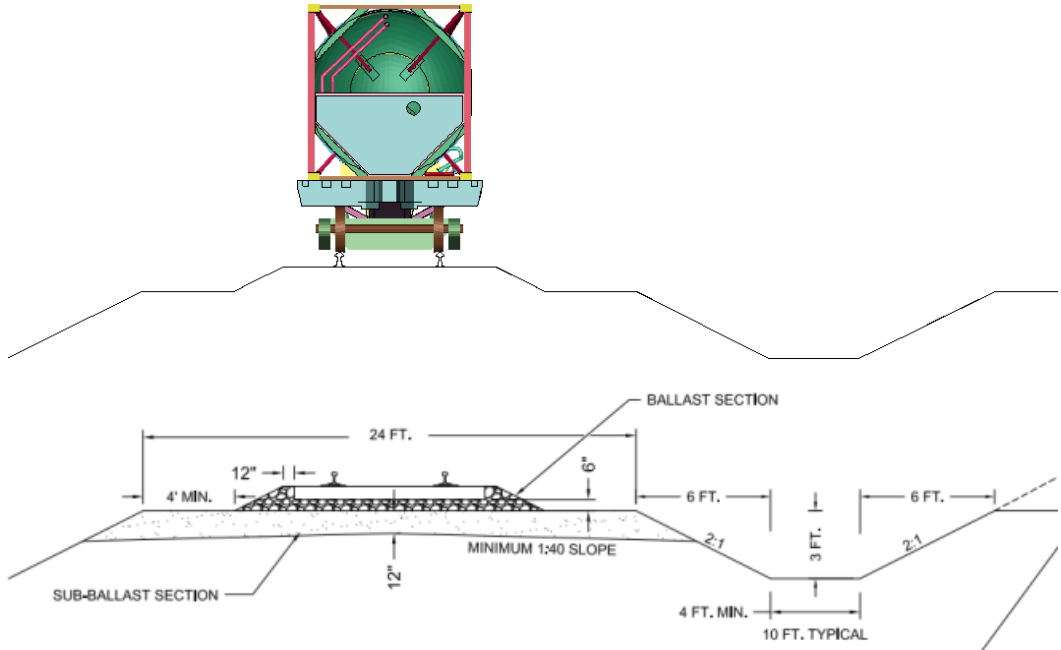
Figure 4. Initial position of vehicle combination including rails, ballast, and surrounding terrain; FE Model (top) and engineering specifications (bottom)
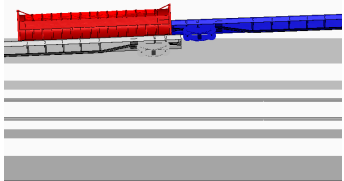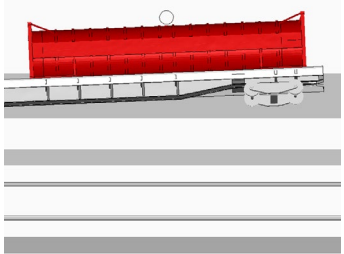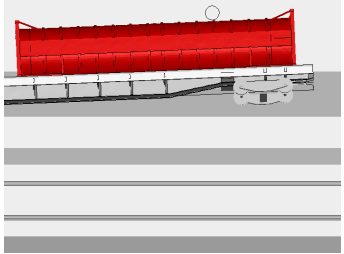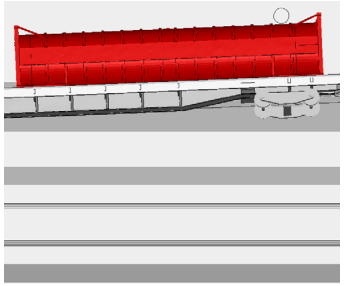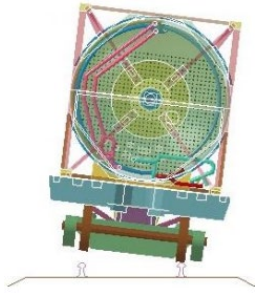
Figure 5. View of model showing LNG within the tank (shown graphically as 'dots') at initiation of rollover

3.2　Methods

Two test series were simulated in this task: a series of crashes and a series of flow tests.

The simulated crash conditions are summarized in Table 2. Each scenario was repeated until the team identified the minimum velocity that resulted in significant damage to the PRV piping assembly to potentially degrade its performance. "Significant" damage was qualitatively defined as deformation of a PRV system component that could result in degradation of the system performance.

11

Table 2. FE Crash Simulation Matrix

Impact Location	Impact Partner	Description
Piping cabinet	Flatcar	Stationary UN-T75 tank & flatcar, rolled 95 deg, is impacted by an empty flatcar
Top Center	24-inch rigid pole	UN-T75 tank and flat car roll into a stationary rigid pole and impact at ~90 deg roll angle at the tank center
Top Third	24-inch rigid pole	UN-T75 tank and flat car roll into a stationary rigid pole and impact at ~90 deg roll angle 13 ft from tank end
Top End	24-inch rigid pole	UN-T75 tank and flat car roll into a stationary rigid pole and impact at ~90 deg roll angle 10 ft from the tank end
Rollover	Rollover	UN-T75 tank and flat car roll off rails onto the surrounding terrain

In flow test simulations, the team modeled the flow of methane gas through a straight length of 2-inch schedule 40 pipe with varying degrees of deformation based on the crash test results. A compressible flow solver was used to account for compression of the gas and its effects on the state of the fluid as it flowed through the pipe. The tests included a baseline case (no pipe damage) and cases with 50, 80, and 95 percent closure.

3.3 FE Results

FE Crash Results are documented in Table 3.

Table 3. FE Crash Results

Mode	Impact Delta-V	Damage
Rear Impact – Flatcar	15 mph	• Exhaust pipe pinched ~50% closed x 2-inch length • Internal tank undamaged
	20 mph	• Exhaust pipe pinched ~80% closed x 19-inch length • Internal tank minor dent
	30 mph	• Exhaust pipe pinched 90% closed x 20-inch length. • Annular space pipe pinched 80% closed x 7-inch length • Internal tank dented
	49 mph	• Exhaust pipe pinched > 95% closed • Exhaust pipe torn • Annular space pipe pinched >95% closed • Annular space pipe torn • Internal tank dented
Top-center – Pole	25 mph	• No pipe damage • Internal tank likely breached
	35 mph	• Internal pipe minimally damaged • Internal tank likely breached
	49 mph	• Internal pipe minimally damaged • Internal tank breached
Top-quarter – Pole	15 mph	• Internal pipe pinched ~50% closed • Internal tank crushed ~25% of diameter
	25 mph	• Internal pipe pinched ~75% closed • Internal tank crushed ~30% of diameter
	35 mph	• Internal pipe pinched > 95% closed with potential tearing • Internal tank crushed ~45% of diameter
	49 mph	• Internal pipe pinched > 95% closed with potential tearing • Internal tank breached
Top-end – Pole	10 mph	• The internal pipe pinched 60% closed • Internal tank crushed ~
	15 mph	• Internal pipe pinched 75% closed with potential tearing • Internal tank crushed ~10% of diameter
	25 mph	• Internal pipe pinched 75% closed with potential tearing • Internal tank crushed ~20% of diameter
	35 mph	• Internal pipe pinched 75% closed with potential tearing • Internal tank crushed ~35% of diameter
	49 mph	• Internal pipe pinched > 95% closed with tearing • Internal tank crushed ~50% of diameter
Rollover	60 deg/s to 180 deg/s	• No notable pipe damage for any of the evaluated rollover conditions

The team observed considerable PRV system data, mostly in the form of pipe damage, in impacts with railcars and rigid poles at speeds as low at 15 mph. No damage to the PRV system directly was noted for any of the pure (i.e., without impacts against other objects) rollover cases up to 180 deg/s roll velocity. PRV system damage was obviously sensitive to the impact location. Longitudinal impacts to the piping cabinet end of the tank caused damage to external, post-PRV piping whereas lateral impacts to the tank resulted in damage to the interior piping assemblies. At 10-15 mph the 2-inch schedule 40 stainless steel pipes were often pinched approximately 50-60 percent closed. Examples of this damage is provided in Figure 6, Figure 7, Figure 8, and Figure 9.
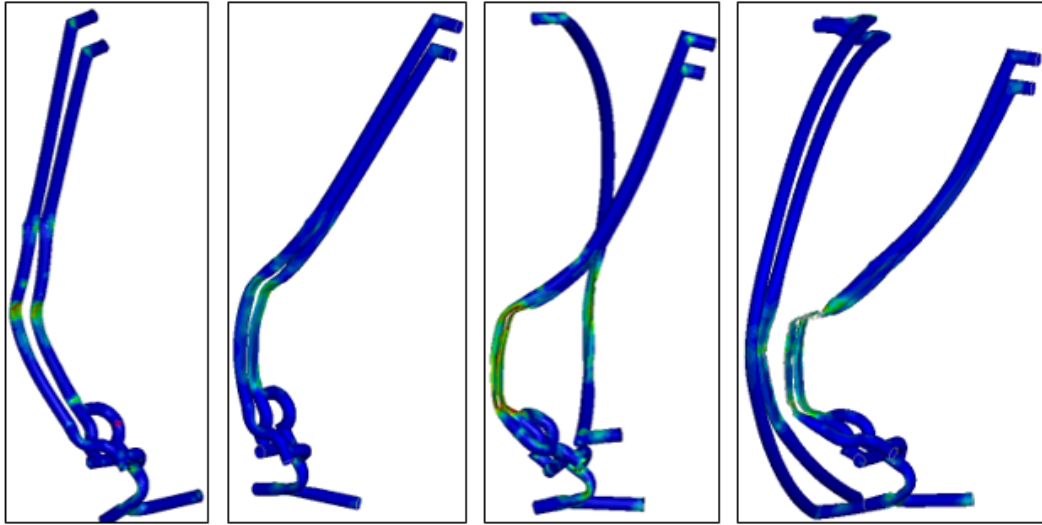
Figure 6 Pipe damage in rear-end flatcar impacts at 15 mph, 20 mph, 30 mph, and 49 mph (from left to right)
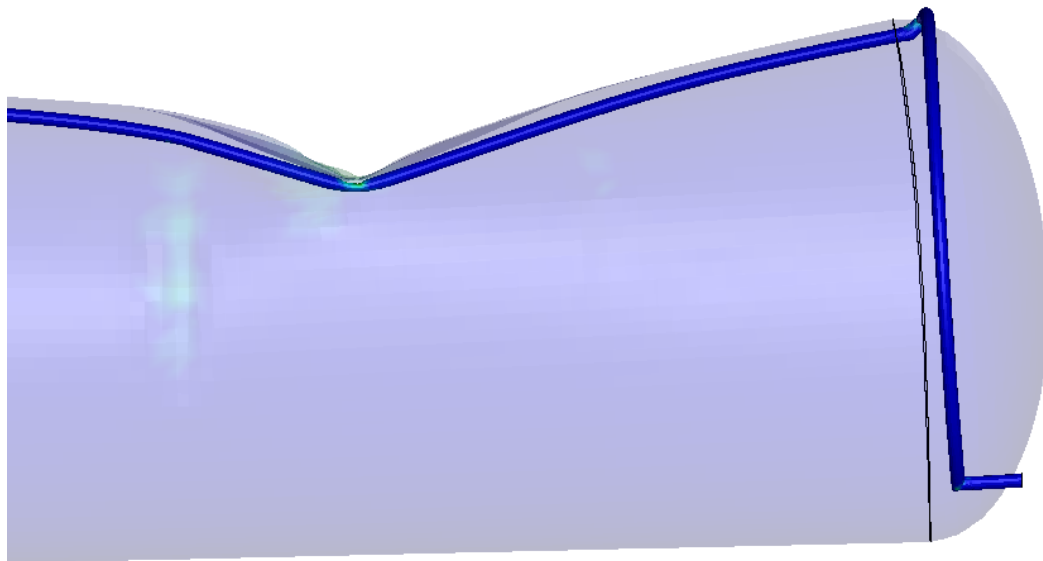
Figure 7. Damage to inner tank and internal PRV piping in the Top-quarter – Pole impact at 15 mph; damage at higher speeds was similar in shape but greater in magnitude

14
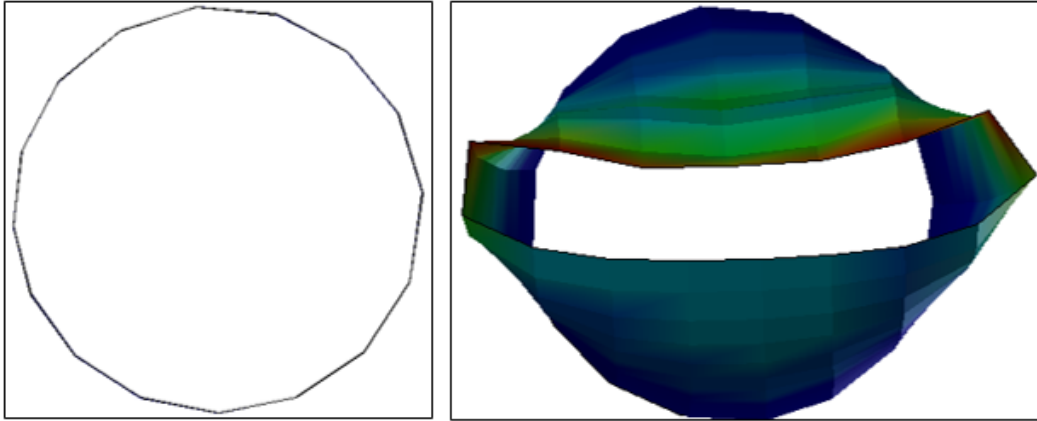
Figure 8. Original (left) and reduced pipe cross-section (right) after 25 mph Top-quarter – Pole impact
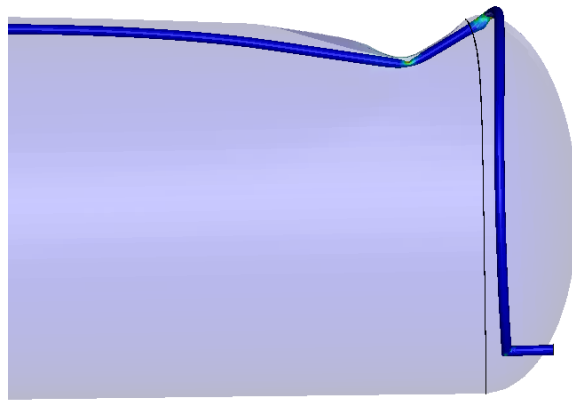
Figure 9. Damage to inner tank and internal PRV piping in the Top-end – Pole impact at 10 mph; damage at higher speeds was similar in shape but greater in magnitude

The flow simulations demonstrated that the damage to the pipes significantly degraded the flow rate (Figure 10). The amount of deformation for each pipe model is shown in Figure 11, Figure 12, Figure 13, and Figure 14. The average velocity through the baseline pipe was 49.5 m/s.
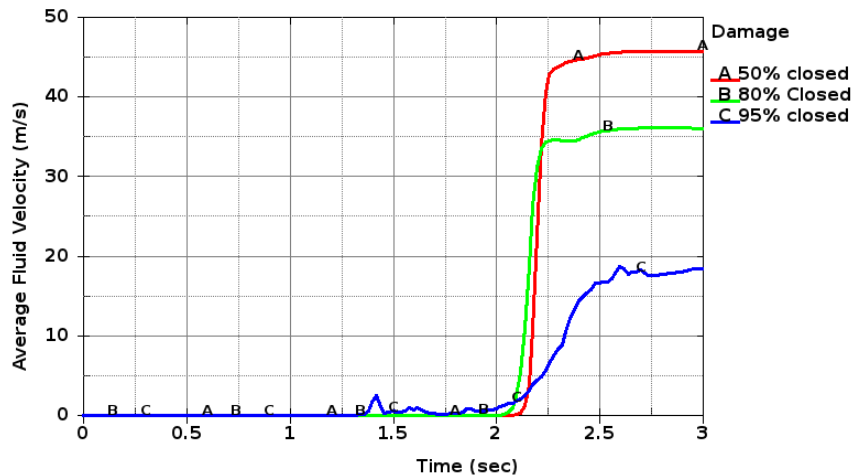
Figure 10. Velocity vs Time for 3 pipe damage severities

15

Pipe Flow
Time =   3.0001
Contours of Fluid_Velocity (magnitude)
min=9.84078, at node#12
max=48.9633, at node#73455
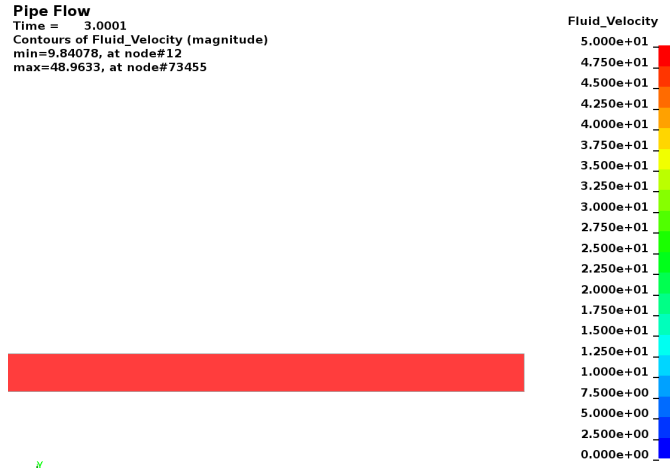
Figure 11. Methane gas flow through nominal pipe at 120 psi inlet pressure
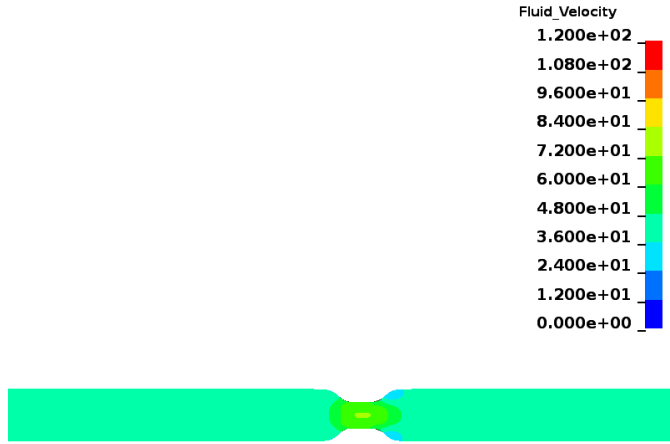
Figure 12. Methane gas flow through ~50% closed pipe at 120 psi inlet pressure
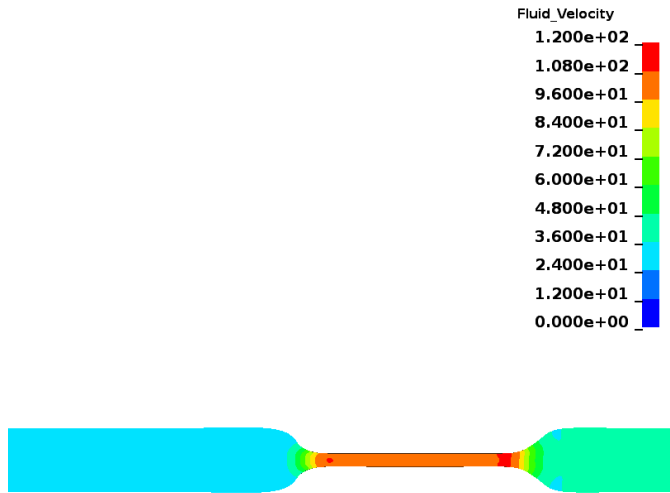
Figure 13. Methane gas flow through ~80% closed pipe at 120 psi inlet pressure

16
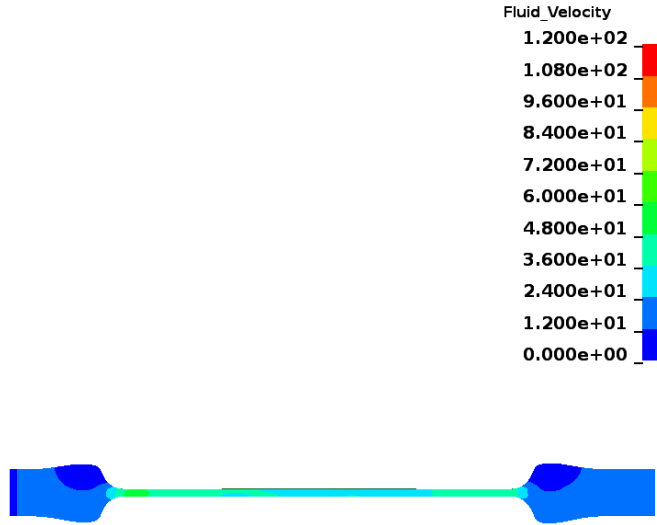
Figure 14. Methane gas flow through >90% closed pipe at 120 psi inlet pressure

3.4 FE Crash Discussion

Deformation of the internal piping assembly (upstream of the PRVs) or external piping assembly (downstream of the PRVs) is possible at impact velocities around 10-15 mph. The extent of piping deformation shown in the FE simulations is likely to degrade the capacity of the assembly to move vapor and/or liquid through the PRV system and is specifically in contradiction to the requirements in 49 CFR 178.274.f.2. The testing described in Section 4 investigated the effect of downstream constrictions on flow rates for cryogenic liquid flow through the PRV and found that flow was substantially reduced.

This study only considered derailment crashworthiness of a specific intermodal tank traveling on top of a flatcar. This represents a particular scenario that exposes the tank to different impact configurations than would be experienced by a tank car or even an intermodal tank double stacked on a well car. These other configurations could be investigated using similar modeling strategies.

4. PRV System Test

Based on the results of the literature review, FE simulations, and previous tests of the UN-T75 tank, the team developed a physical test matrix to characterize the flow rate of cryogenic liquid nitrogen through a representative PRV assembly. The testing series included varying the inlet pressure, downstream constriction, PRV temperature, and environmental conditions (e.g., temperature and humidity). Measured output responses included mass flow rate, fluid and PRV temperature, and fluid density.

4.1   Test Methods

The research team, working with Southwest Research Institute (SwRI) with input from FRA, designed and constructed an experimental PRV testing system using the 6,000-gallon LN2 vessel that provides nitrogen supply to SwRI's Flow Component Testing Facilities. The PRV testing system was developed by 1) constructing the plumbing and controls for the LN2 (cold side) supply from an existing valve on the bottom of the LN2 supply vessel, and 2) creating a nitrogen gas charge system (gas side) to inject gaseous nitrogen into the head space of the LN2 supply vessel to provide gaseous nitrogen to the PRV inlet. This system allowed the team to deliver liquid nitrogen to the PRV from the cold side at controlled headspace pressure supplied from the gas side. In addition, gaseous nitrogen could be supplied to the isolated upstream side of the PRV after an LN2 discharge to check for any gaseous leakage around the seat. A drawing of the PRV testing system is provided in Appendix A. The size and pressure rating of the LN2 vessel provided sufficient volume to meet and exceed the estimated PRV discharge capacity. The large LN2 storage volume allowed more than sufficient flow time for flow discharges beyond one minute in duration.

4.1.1   Test Articles (PRVs)

The team used Rockwood Swendeman 710NEGH-A114 PRVs in this experiment, specifically RXSO bronze ASME coded bodies with a 2-inch orifice, 1.5-inch inlet diameter, and 2-inch outlet diameter. These are the same model numbers used on previous UN-T75 tests and represent the most common design used on similar tanks. The A114 indicates that it is intended for air or gas service with a set pressure of 114 psi. The PRV was sealed with a metal seat and PTFE plunger.

4.1.2   Test Section

The test section piping arranged for PRV testing was fabricated per the test section and setup fabrication drawing shown in Appendix B; the test setup CAD model is shown with additional content in Figure 15. The test section included 2-inch schedule 40 304L stainless-steel piping, a 1-inch full bore automated cryogenic ball valve on the upstream side (upstream supply isolation valve), a 2-inch Coriolis flow meter, and a tee with a 1-inch full bore automated cryogenic ball valve used as a purge to atmosphere (i.e., purge valve) located just upstream of the PRV. Ports to measure pressure and temperature were located upstream of the flow meter and upstream of the PRV. The official upstream pressure measurement was taken at three nominal pipe diameters (3D) upstream of the PRV connection. A 1.5-inch diameter stainless-steel hose connected the LN2 supply vessel to the upstream supply isolation valve.
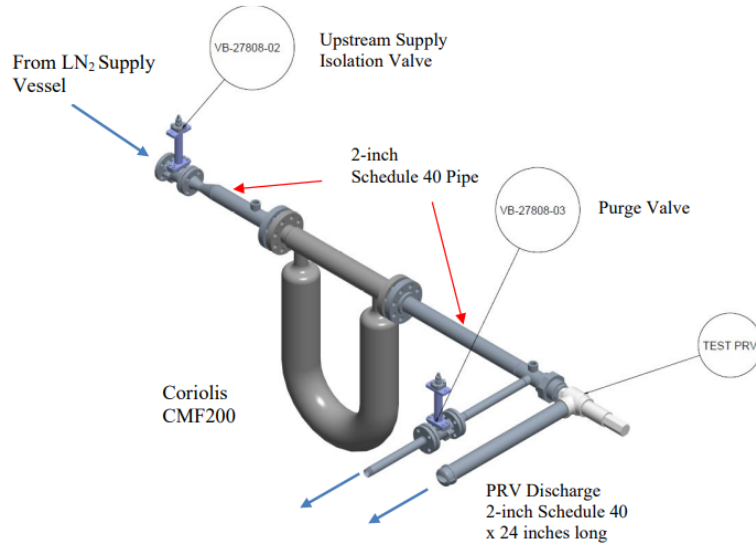
Figure 15. PRV test section arrangement

Testing was performed using the system as shown in Figure 16.
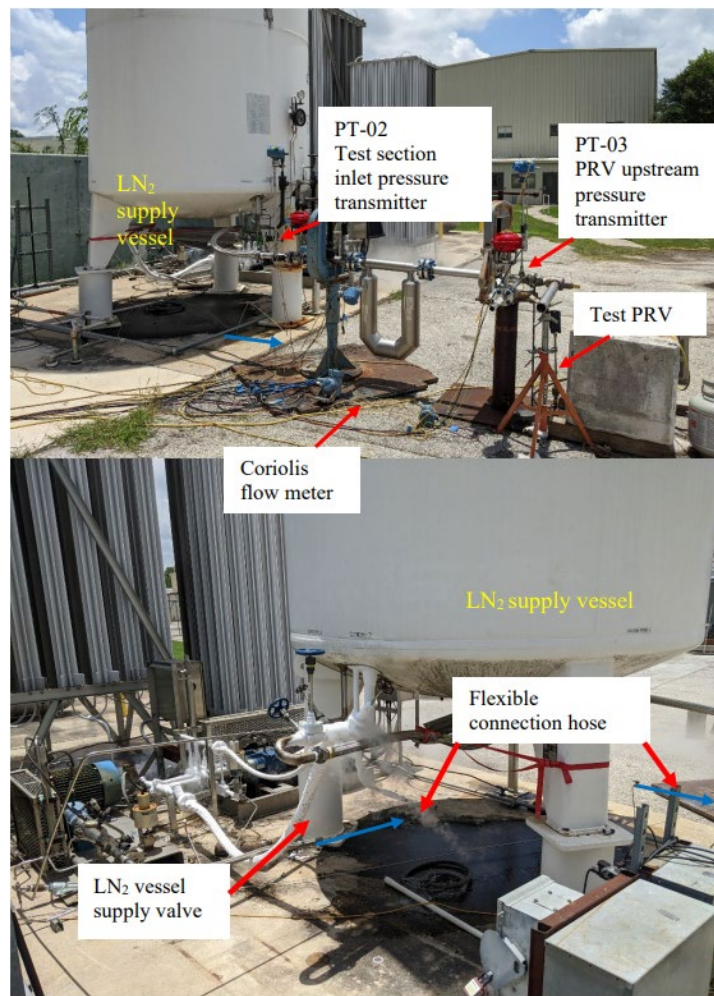
Figure 16. PRV test system

The figures show the LN2 supply plumbing and testing instrumentation. The pressure transmitters were mounted on vertical static stand-off tubes used to isolate the pressure transmitter diaphragm from the cryogenic temperature. High-accuracy Rosemount 3051S smart transmitters were used to measure pressure, and a Micro Motion ELITE CMF200 Coriolis flow meter was used to measure the mass flow rate of the nitrogen and the nitrogen fluid density. Type K thermocouples were used to measure the PRV temperature, and the fluid temperature measured upstream of the flow meter. All test data were measured and recorded electronically using an existing facility data acquisition system. This data acquisition and control system was also used to control the upstream supply valve and purge valve remotely from the facility control room.

4.1.3 Nitrogen Gas Charge System

The nitrogen gas charge system is also shown in the test system piping and instrumentation diagram (P&ID) in Appendix B. Gaseous nitrogen supplied from SwRI's nitrogen source (pressure-stored at 2,000 - 2,900 psig) was used by reducing pressure through a pressure regulator to inject the nitrogen and increase the pressure in the 6,000-gallon LN2 supply vessel. A pressure transmitter was used on the gas injection line to measure the LN2 supply vessel pressure. Gas was injected until the desired test run start pressure was reached. A small diameter (1/4-inch tubing) supply line containing an isolation valve branched from the LN2 injection line and connected to the upstream PRV pressure port location on the test section. This line was used to apply ambient temperature gaseous LN2 into the test section for PRV seat testing. The pressure-reducing regulator was used to control the pressure.

4.1.4 PRV Discharge Piping Arrangement

A 2-inch schedule 40 pipe measuring 24-inches-long was used as the PRV discharge plumbing for the initial series of tests. A second series of tests added two 90 deg elbows and 12 ft of 2-inch piping downstream of the original discharge assembly (Figure 17). This was done to more closely replicate the total length of piping downstream of the PRV assembly on a UN-T75 tank.
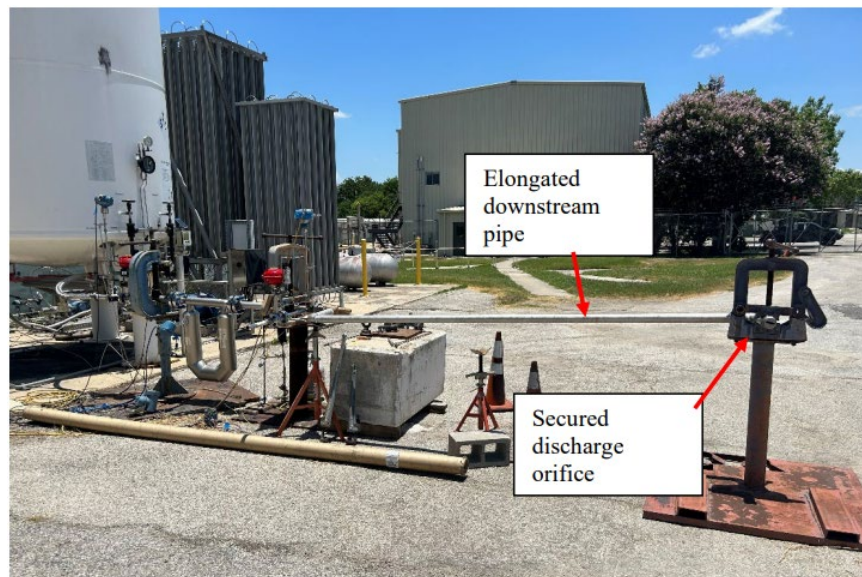
Figure 17. PRV test system longer discharge

A PRV discharge piping constriction, used for certain tests, was created by machining elliptical-shaped orifices in a 2-inch pipe cap to replicate a crushed (i.e., oval-shape) pipe. The two PRV discharge-constricted orifice sizes with which the PRV was tested are shown in Figure 18. The orifice area on the more severe constriction is 0.785 in^2 which represents an 89 percent closure. The orifice area on the less severe constriction (1.57 in^2) represents a 78 percent closure.
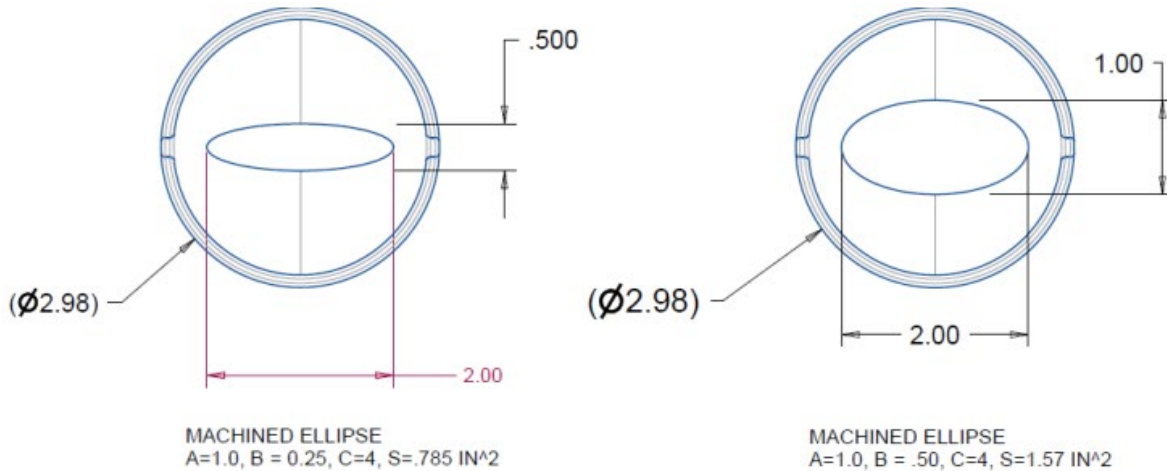
Figure 18. Machined elliptical orifices used for PRV discharge constriction

4.1.5 Simulated Fire Test

A 500,000-BTU propane torch was used to heat the PRV to simulate rapid heating of the PRV during a crash scenario. The PRV body temperature was monitored with a Type K thermocouple strapped to the body with a ring clamp. The propane torch was modified for safe operation and remote control by placing a control valve on the propane feed and equipping the torch with an electric igniter.

4.1.6 Test Series Description

All tests were conducted with pressurized LN2 applied at the inlet of the PRV test section. The test matrix (Table 4) was developed based on the cause-and-effect analysis that is summarized in Table 1 to quantify the effects of potential PRV degradation scenarios.

Table 4. PRV Flow Test Matrix

	Pressure (psi)	Constriction	Relative Humidity	PRV Temperature (°F)
Baseline	130, 150, 190	None	Ambient	Ambient
Constriction	130, 175, 190	78%, 89%	Ambient	Ambient
Heated	130, 240	None	Ambient	721, 744, 1000
Humid	130, 150	None	80-100%	Ambient
Extended exhaust	130, 180	None	Ambient	Ambient
Extended exhaust + constriction	130, 180	89%	Ambient	Ambient

The primary degradation scenario of interest was the effect of cryogenic liquid flow through the PRV assembly. The key test parameters included cryogenic fluid flow to represent the PRV inlet no longer in the vapor space, elevated PRV temperature to simulate damage to seals, and constricted outlet piping to simulate increased backpressure. Tests at increased ambient humidity were performed to replicate the conditions that led to PRV ice-up in previous tests. Test conditions were repeated multiple times and data was collected in each test for at least 60 seconds or until equilibrium was achieved. Testing revealed some sensitivities such as the effect of the LN2 supply tank fill level that affected test outcomes in an unexpected manner.

4.2   Test Results

For each test, the temperature was recorded both upstream of the Coriolis flow meter and at the PRV. Pressure was monitored and recorded upstream of the Coriolis flow meter on the gaseous nitrogen feed into the headspace and just upstream of the PRV. Mass flow rate and fluid density were monitored by the Coriolis flow meter and recorded. For ease of viewing the data in this section, the PRV temperature and pressure, as well as the mass flow rate and the fluid density, are shown as a function of time.

4.2.1 Baseline Tests

The baseline tests consisted of repeatedly discharging LN2 through the PRV at a headspace pressure ranging from 130 to 190 psi. During the baseline tests, two feet of 2-inch pipe were connected to the downstream discharge from the PRV with no constrictions added. Figure 19 shows a typical discharge experiment. This run happens to be at 130-psi drive pressure, and it is the first discharge in a sequence. So, it can be observed that the PRV temperature starts close to 100°F before rapidly dropping to cryogenic temperatures.

Figure 19. Baseline test at 130 psi – Run 1 (PRV temperature [°F], PRV pressure [psi], mass flow rate [lb/min], and density [kg/m³])

As can be seen, it took over one minute for the PRV to cool to equilibrium, and subsequently, it took as long for the flow rate and fluid density to equilibrate. Conversely, on a repeat discharge experiment, the PRV was pre-cooled and the system reached equilibrium much more quickly (approximately 15 seconds), as shown in Figure 20.
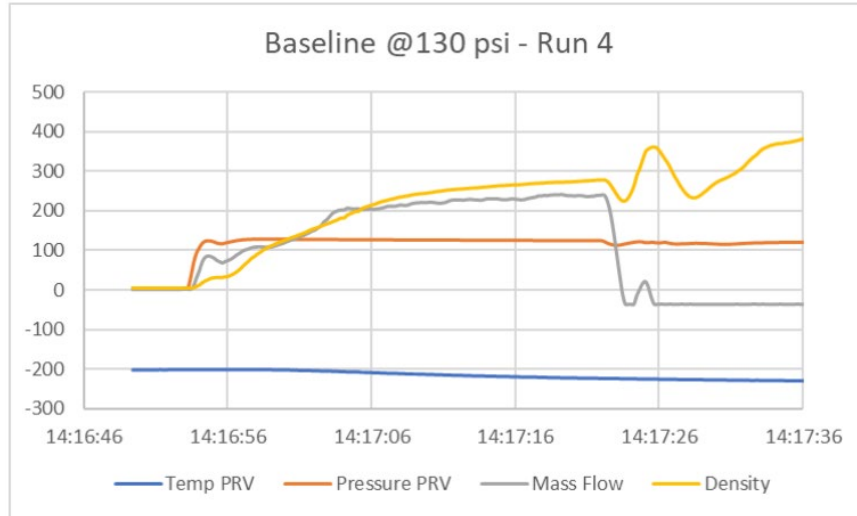
Figure 20. Baseline test at 130 psi – Run 4 (PRV temperature [°F], PRV pressure [psi], mass flow rate [lb/min], and density [kg/m³])

This process was repeated at several discharge pressures. In all cases, it was observed that upon closing the upstream control valve to terminate LN2 flow, the PRV reseated and held pressure. This can be seen in the orange PRV pressure traces in Figure 19 and Figure 20.

A summary of equilibrium mass flow rates as a function of discharge pressure for the baseline tests is plotted in Figure 21.
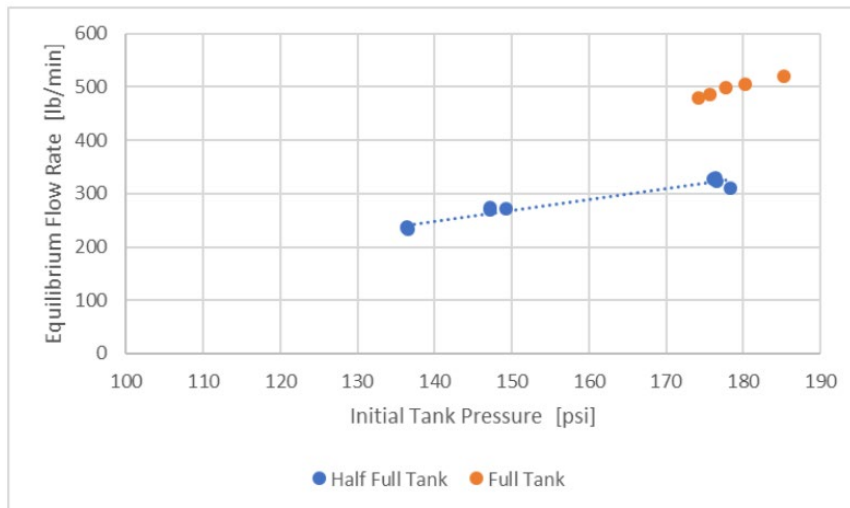
Figure 21. Summary of baseline tests – Flow rate vs. tank pressure

The mass flow rates recorded in these tests were similar to the mass flow rate generated from high pressure (~870 psi) natural gas leaking through a 20 mm diameter orifice (Lowesmith & Hankinson, 2012). The most surprising feature of these data is that the flow rate was not dictated solely by the upstream pressure. It was only discovered after plotting the data that the mass flow rate increased significantly after a regularly scheduled filling of the LN2 supply tank was completed, even at similar upstream pressures. The cause of this increase became clear once the liquid density was plotted in a similar manner (see Figure 22). It was discovered that the density of the fluid discharged through the Coriolis flow meter had significantly increased. In the tests

prior to the LN2 resupply, the fluid density indicated a two-phase flow was entering the Coriolis meter. After resupply the flow was at a density indicating it was nearly pure liquid. Not only does an increase in fluid density help drive higher mass flow rate, but it also mitigates the choked flow issue that is likely associated with the two-phase flow condition.
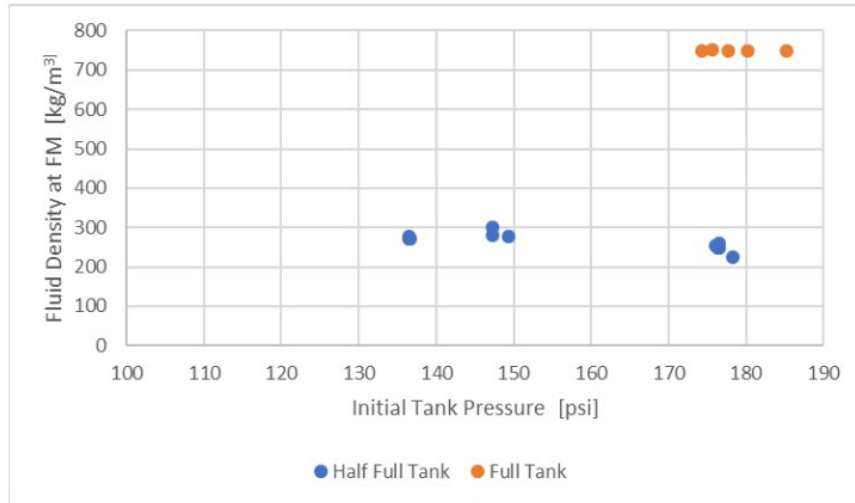
Figure 22. Summary of baseline tests – Fluid density vs. tank pressure

4.2.2 Constriction Tests

The research team also studied the effect of a constriction on the downstream discharge tubing to simulate a bent or partially pinched pipe downstream of the PRV. Two different sizes of orifices were cut into pipe end caps to repeatedly simulate this type of constriction. Once again, the PRV was able to safely discharge and reseat in all of the tests. The summary of the results of these tests is shown in Figure 23.
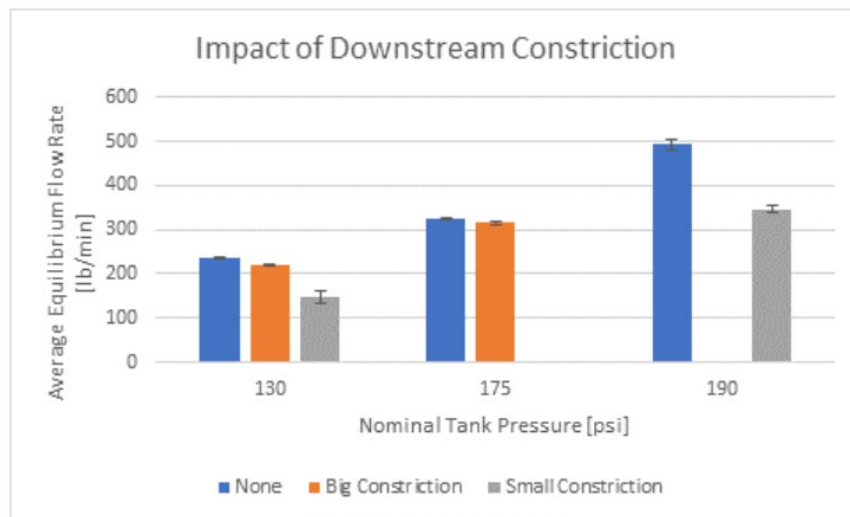
Figure 23. Comparison of unrestricted vs restricted downstream conditions; note that the 130- and 175-psi discharges were conducted with the supply tank half full, and the 190-psi discharges were conducted immediately after the supply tank was filled

24

The high-pressure data for the 78 and 89 percent constrictions cannot be directly compared because the supply tank was filled while conducting this testing. The impact on the results was not fully understood until after the data were processed. Even with this limitation, a consistent trend was observed in that the 78 percent downstream constriction resulted in very little flow rate decrease (approximately 3.5 to 5.5 percent). The 89 percent downstream constriction resulted in a much more significant decrease in mass flow rate, for both the two-phase fluid flow at 130 psi and the nearly single-phase liquid flow at 190 psi. A decrease of approximately 30 to 38 percent was observed for the smaller constriction. In addition to the reduction in equilibrium flow rate, the flow rate oscillated considerably upon initial opening of the PRV. This can be observed in the example trace shown in Figure 24.
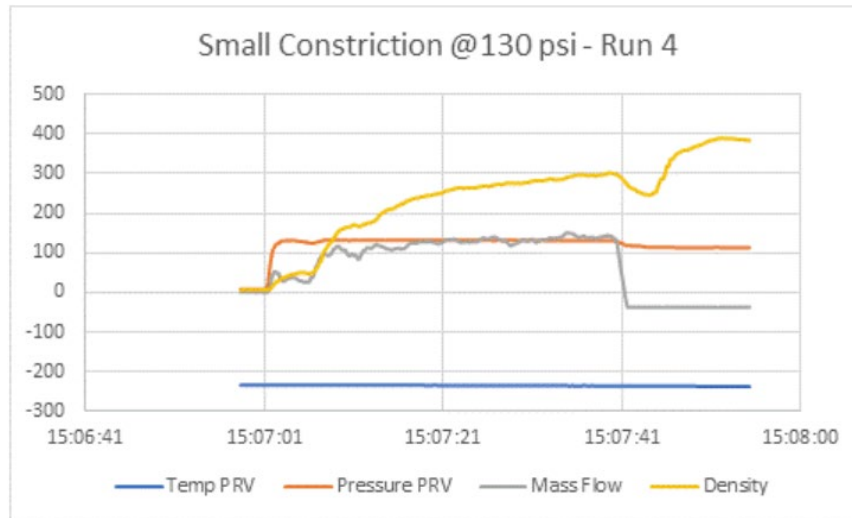
Figure 24. 89% Constriction at 130 psi – Run 4 (PRV temperature [°F], PRV pressure [psi], mass flow rate [lb/min], and density [kg/m^3])

This oscillation in the flow rate occurs because upon initial release, the downstream orifice creates backpressure in the discharge piping. The result is that the differential pressure across the PRV decreases, and it begins to shut. As the PRV chokes off, the flow rate decreases and, consequently, so does the backpressure in the downstream pipe. The result is that the PRV reopens fully.

4.2.3 Heated Tests

This section summarizes the results of preheating the PRV to high temperatures to simulate a nearby fire or other heat source. This was accomplished by using a propane torch to preheat the valve and then discharging LN2 through the PRV. Whenever the PRV was heated above approximately 700°F for a significant time, the PTFE plunger in the PRV melted or thermally decomposed causing a failure in the ability of the PRV to reseat and hold pressure. The PRV still opened successfully, but it no longer functioned as a pressure relief valve with a set pressure.

An example plot of a hot test is shown in Figure 25 where the mass flow rate reached 800 kg/m^3 for a tank pressure of 240 psi. The PRV failed its seat leakage test after any hot test above 700°F. The loss of the PTFE plunger due to thermal effects resulted in a slight increase in mass flow rate (approximately 14 percent higher) as compared to experiments where the PTFE was undamaged.
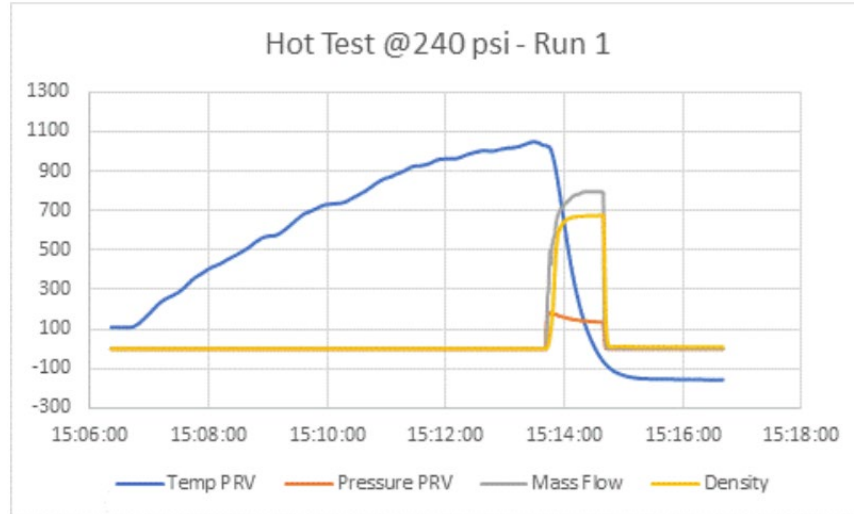
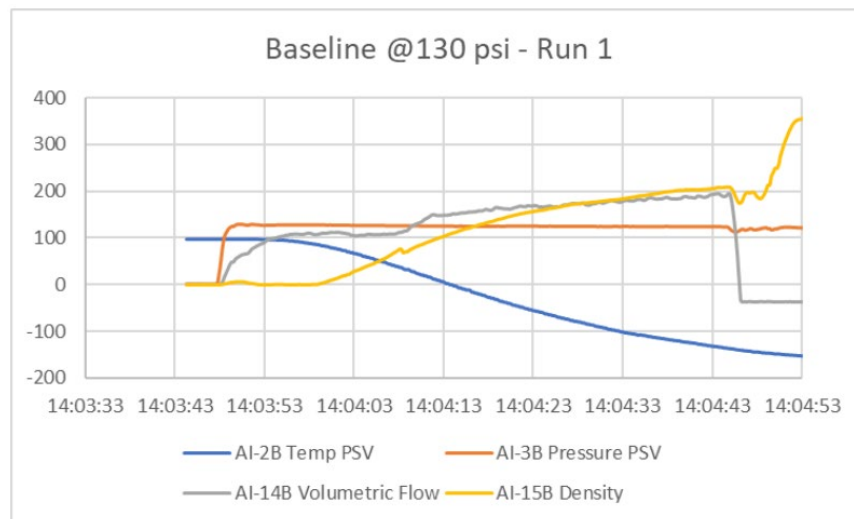**Figure 25. Hot test at 240 psi – Run 1 (PRV temperature [°F], PRV pressure [psi], mass flow rate [lb/min], and density [kg/m³])**

Tests were conducted just below 721°F, just at 744°F, and above 1050°F, the melt temperature of the PTFE seal. In the case of heating to below the melting temperature of the PTFE, the seat swelled slightly but it did not cause the PRV to fail to open or affect its performance. In the case of heating to just at the melting temperature of PTFE, it was observed that while the PRV had no issues opening, the flow rate was much more unstable (see Figure 26).
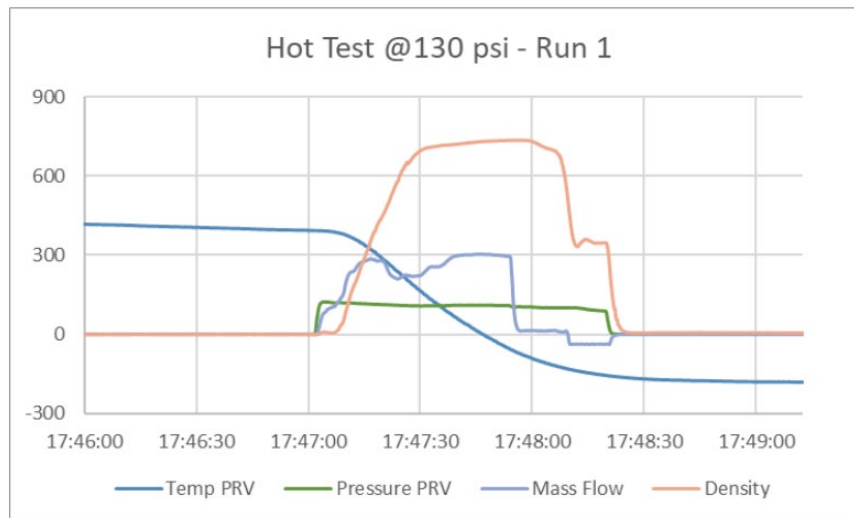
Figure 26. Hot test at PTFE melt temp (PRV temperature [°F], PRV pressure [psi], mass flow rate [lb/min], and density [kg/m³])

The pressure at the PRV decreased slightly over time and the PRV failed the subsequent seat leak test. It is unclear if this valve would have functioned properly if another LN2 discharge was attempted after sustaining this damage. The springs on the PRVs that reached more than 1,000°F were permanently compacted slightly, and it is unclear if the PRV would have been able to reseat correctly even if the PTFE had not been completely removed. It is suspected that a softening of the spring occurred while being compressed at high pressure, and it remained compressed while

the LN2 quenched the spring in this compressed position. The thermal damage to each of the PRVs can be seen in Figure 27.
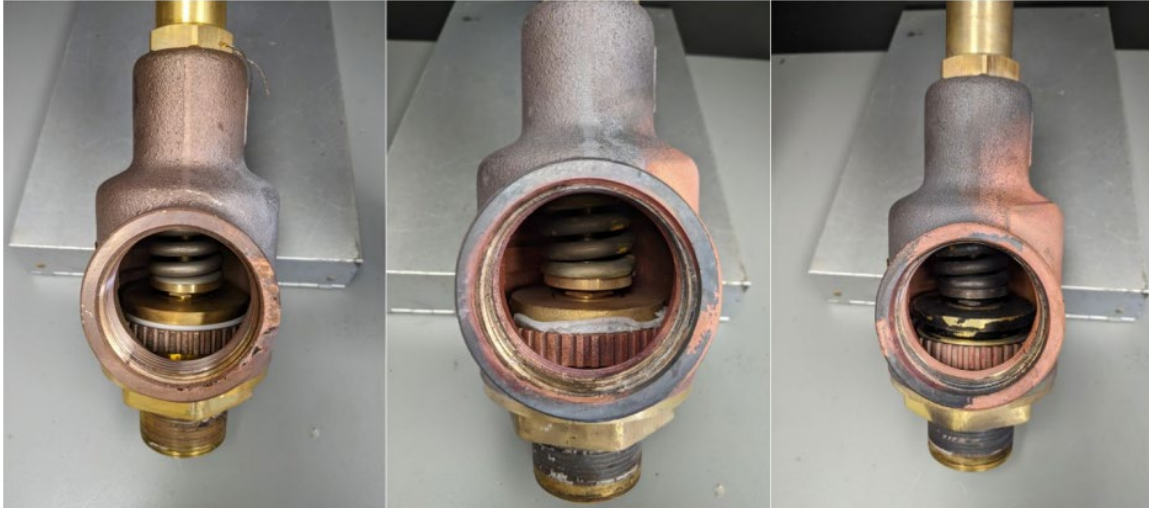
Figure 27. PRVs after hot testing; temp < melt (left), temp = melt (middle), temp >> melt (right)

4.2.4 Humid Tests

The relative humidity at the test facility on multiple occasions during testing reached 80 to 95 percent. Several tests were conducted at high humidity to determine if the PRV would ice over or fail to reseat due to ice buildup from ambient moisture in the air. In these tests the PRVs were precooled for 2 to 10 minutes down to a temperature approaching -220°F and with discharges of several minutes. One such test is shown in Figure 28.
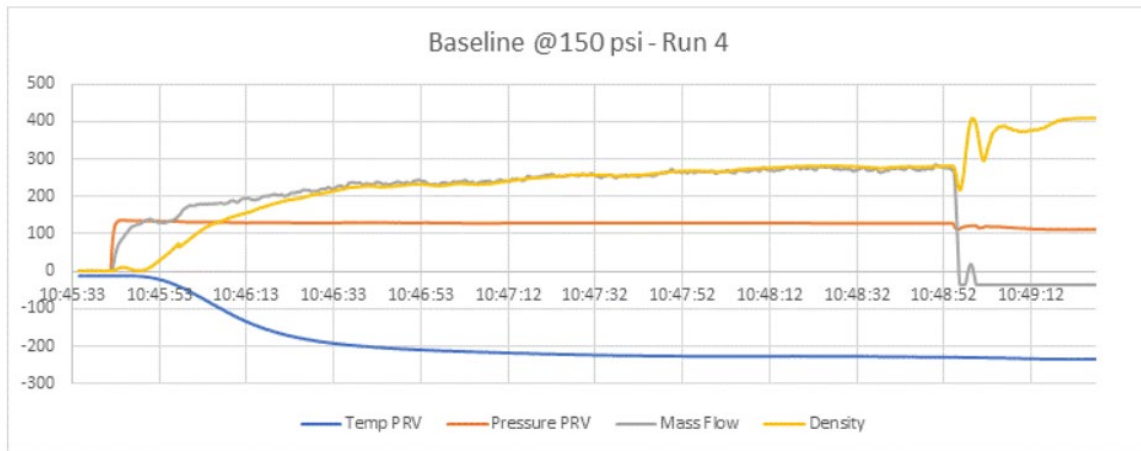

Figure 28. Humid test at 150 psi – Run 4 (PRV temperature [°F], PRV pressure [psi], mass flow rate [lb/min], and density [kg/m³])

Significant ice buildup was seen on the external PRV body, as well as on all the piping. However, due to the downstream discharge piping, the moisture and ice could not build up on the internal components of the PRV. Even at near-saturated humidity, the volume of air in and around the PRV internals did not hold sufficient moisture to build up and restrict the PRV mechanism. In all the humid tests the PRV reseated, sealed, and held pressure.

4.2.5 Extended exhaust

The baseline tests were repeated with the addition of an extended exhaust pipe assembly that included two 90-degree angles and 12 ft of pipe to more closely replicate the total length and quantity of fittings on the fire-tested UN-T75 tank.

Three tests of multiple discharges were executed: 130 psi (tank full), 130 psi (tank half full), and 175 psi (tank half full). The first of the baseline tests was performed with a tank head pressure of 130 psi, but only two of the five discharges were completed. The LN2 supply vessel was almost full of liquid, meaning that the built-up head pressure was quickly spent, and significant time was needed to allow it to rebuild. It should be noted that LN2 had been freshly supplied to the vessel, so it had no time to equilibrate its temperature. In the second baseline test the head pressure was once again 130 psi, but the supply vessel was approximately half full. A large quantity of fluid had been pumped into separate storage tanks a few hours before the test and time was allowed for the fluid to equilibrate in temperature. A full five discharges were conducted for the baseline test, and a further five were performed with the same head pressure and tank conditions, but with the constricted orifice installed.

The results were comparable to the original tests with shorter exhaust length, as shown in Figure 29.
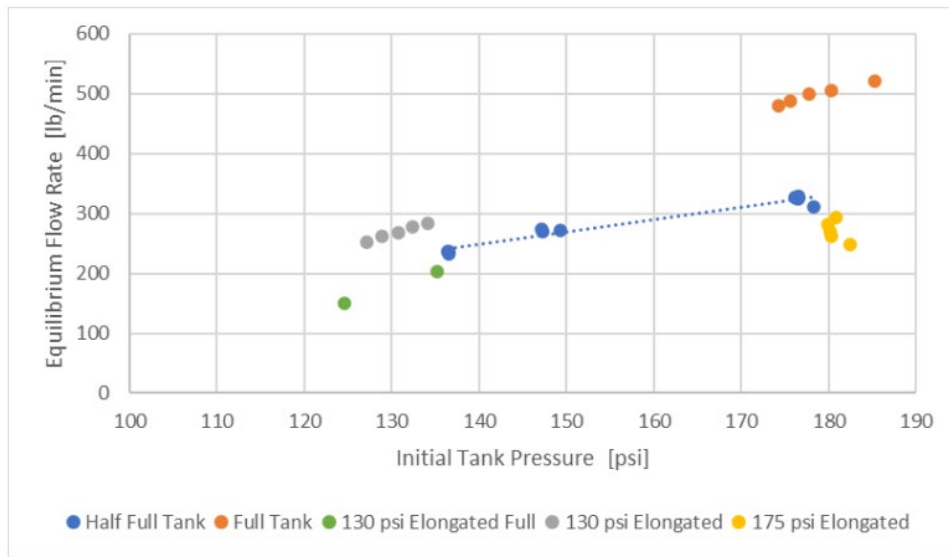
Figure 29. Summary of mass flow rates with extended exhaust added

The 130 psi and 175 psi tests were repeated with the addition of the more sever constriction which represents an 89 percent closure of the pipe. Again, the results were similar to the baseline conditions as shown in Figure 30.
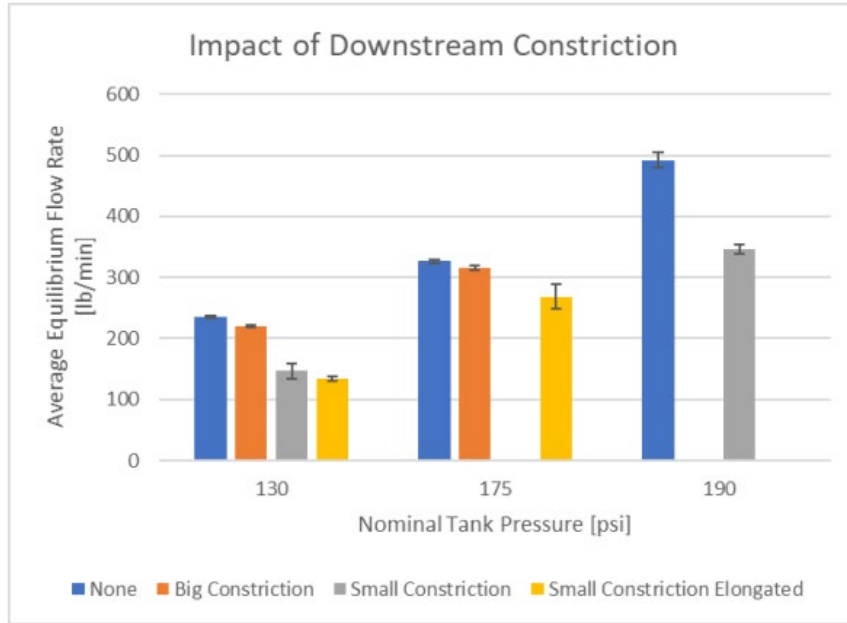
Figure 30. Summary of mass flow rates with extended constricted exhaust added

5. PRV Exhaust Flame Test

The thermal characteristics of natural gas flares/jet flames were quantified through a series of physical tests at SwRI's Fire Technology Department. The objective of the testing was to generate thermal data for different configurations, flow rates, and pressures that can be used to investigate the effects on the thermal response of rail tanks and to use in the validation of future simulations (e.g., Fire Dynamics Simulator).

5.1 Test Methods

5.1.1 Facility Overview

Testing was conducted in a large-scale steel-lined facility nominally 65 x 65 x 60 ft. An adjustable 55 x 55-ft false ceiling allows simulating structures of different heights; for this project it was raised to its full height. Combustion air enters the building through 12 symmetrically placed louvers around the perimeter of the building. The twin exhaust fans (each capable of moving up to 60,000 scfm of air) are operated during test runs to allow for quick and efficient smoke extraction.

Tests can be viewed from an exterior door and an elevated observation room adjacent to the building or directly from the test floor, depending on the project scope. The facility also houses the data acquisition system, control system for exhaust cans, and fire suppressant system. Figure 31 shows a basic schematic of the test facility site.
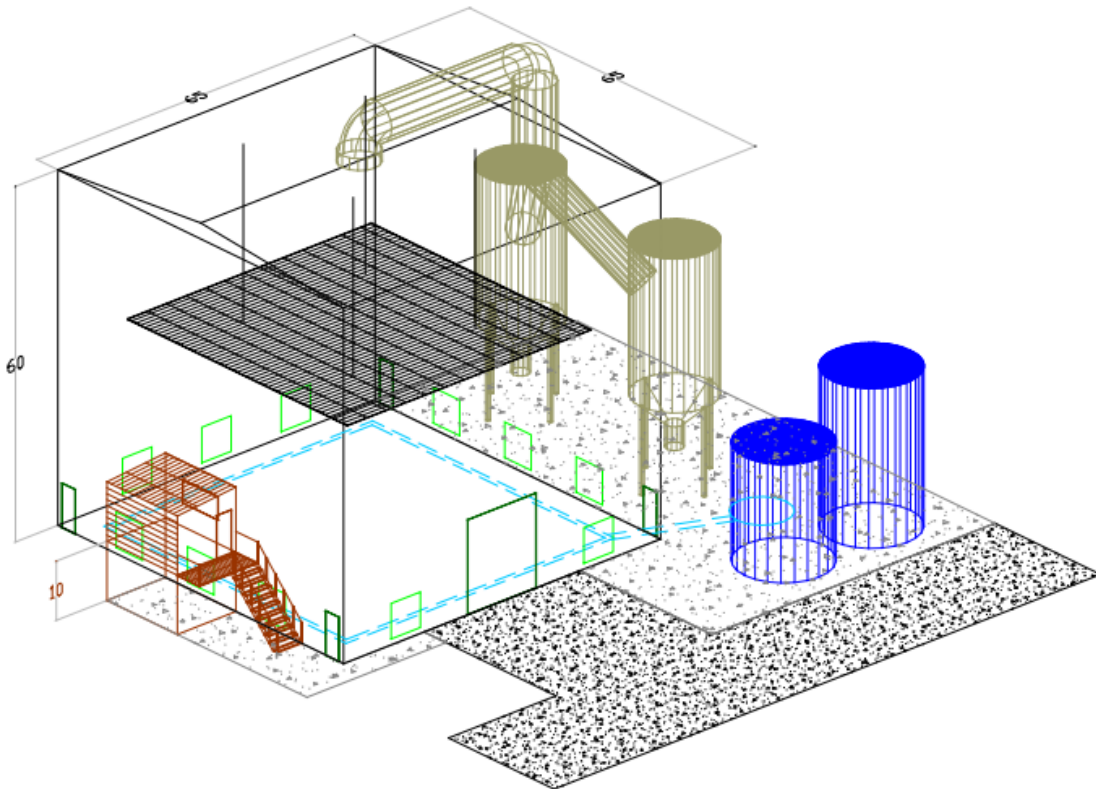
Figure 31. Large-scale fire engineering and research facility layout

5.1.2 Test Setup

Figure 32 shows a general schematic of the test setup for the NG delivery to the ignition source (i.e., propane gas sand burner). All piping used in the setup was schedule 40. The natural gas supply was 96.3 percent methane, 1.7 percent nitrogen, 1.6 percent ethane, 0.2 percent carbon dioxide, 0.1 percent propane, and 0.1 percent additional trace compounds (i.e., light hydrocarbons). Based on the measured constituents, the weighted-average heat of combustion was calculated to be 48.99 kJ/g.
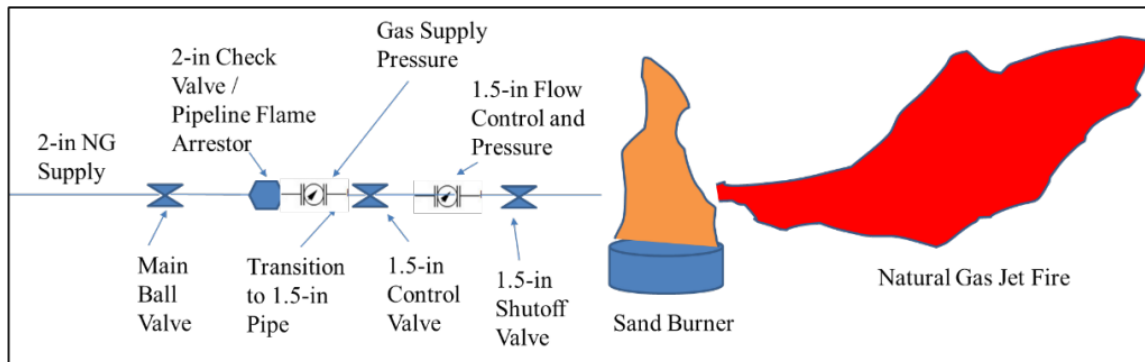
Figure 32. Schematic of natural gas delivery piping setup

Two measurement stations were set up at specified distances from the visually observed flame top or flame middle position of the jet fire and provided room temperature and heat flux at three elevations (1.5, 4.5, and 7.5 ft above the floor; the NG pipe was 2 ft above the floor).

Figure 33 provides schematics showing the relative position of the instrumentation stations for the horizontally oriented jet fire tests. Figure 34 shows a schematic of the relative position of the instrumentation for the vertically oriented jet fire tests.
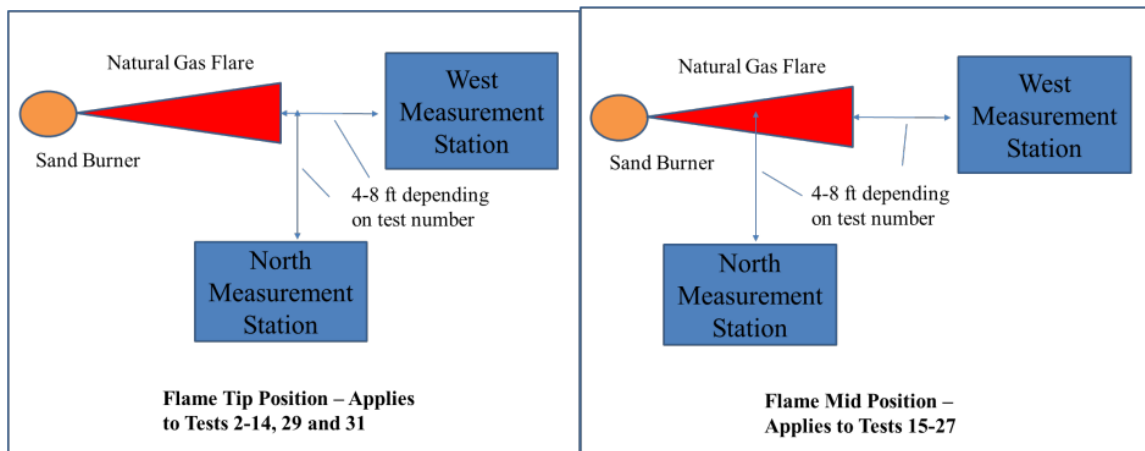
Figure 33. Schematic of instrumentation stations for horizontal jet fire tests

Temperature was measured from 20-ga Type K thermocouple wire (Geocrop model K20-2-G). Heat flux was measured from Schmidt-Boelter heat flux transducers with a range of 0-50 kW/m^2 (Medtherm model 64-5-19 or 64-5-20). The 2-in diameter line pressure was measured with a pressure transducer with a range of 0-200 psig (Honeywell model THE) and the downstream discharge pressure was measured with a 0-100 psig range transducer (Tecsis Model 99-6702-100G). The discharge flow rate was measured with a flow controller with a range of 0-3000

31

SLPM (Omega model FMA-2323-V2). All instrument outputs were logged on a data acquisition SYSTEM (Yokogawa model DU-100-11) at 1 Hz.
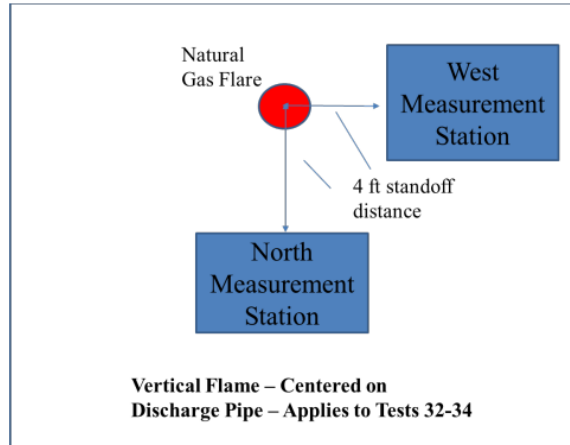
Figure 34. Schematic of instrumentation stations for vertical jet fire tests

The following nominal test procedure was used for each run.

1. Ignite the sand burner (pilot)

2. Start DAQ

3. Open main valve

4. Adjust line flow rate and/or pressure.

5. Flow for two minutes and collect data.

6. Close main valve and reset for next test

The summary data that is provided in this report is average data over the last 30-120 seconds of each run at a given configuration. Additional discussion of post-processing is provided in the test results section of this report. Figure 35 shows two photographs of the setup for the natural gas supply line and instrumentation to measure flow rate and line pressure. Figure 36 shows two photographs of a representative test before and after ignition of a jet fire flame.
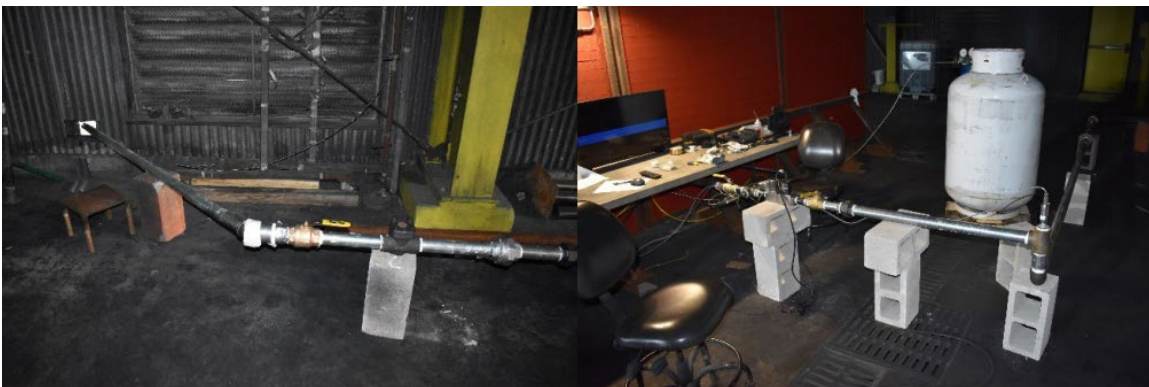
Figure 35. Natural gas supply into test facility, main cutoff valve, check valve and pipeline flame arrestor (left); Transition to 1.5-in diameter pipe and pressure flow rate measurement to data acquisition system (right)
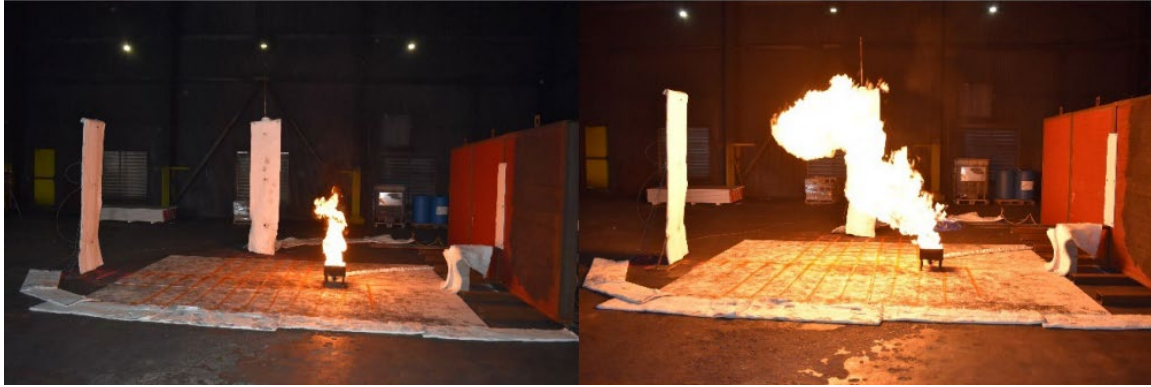
Figure 36. Pre-test conditions after sand burner is ignited (left); Test in progress with jet flame and north measurement state at mid-flame position (right)

5.1.3 Test Plan

The general plan included running tests across a range of natural gas flow rates and recording heat flux and temperature at two measuring stations (North and West). Table 5 provides the full test matrix.

Table 5. Summary of jet fire test matrix

Test No	Flow Rate (SLPM)	Standoff Distance (ft)	North Station Flame Position	North Distance to Discharge Pipe (ft)	West Distance to Discharge Pipe (ft)	General Description / Additional Comments
1	3000	~4	~Tip	ND	ND	Scoping test to find position
2*	3000	4	Tip	7.5	11	First official test
3	3000	4	Tip	7.5	11	Repeat last test
4	2500	4	Tip	6.5	10	Changed flow rate
5	2000	4	Tip	5.5	9	Changed flow rate
6	1500	4	Tip	4.5	8	Changed flow rate
7	1000	4	Tip	3.5	7	Changed flow rate
8	500	4	Tip	1.5	5.5	Changed flow rate
9	3000	8	Tip	7.5	15	Changed standoff distance
10	2500	8	Tip	6.5	14	Changed flow rate
11	2000	8	Tip	5.5	13	Changed flow rate
12	1500	8	Tip	4.5	12	Changed flow rate
13	1000	8	Tip	3.5	11	Changed flow rate
14	500	8	Tip	1.5	9.5	Changed flow rate
15	3000	4	Mid	3.75	11	Changed station position
16	2500	4	Mid	3.75	10	VOID, forgot to move station
17	2500	4	Mid	3.25	10	Repeat test
18	2000	4	Mid	2.75	9	Changed flow rate
19	1500	4	Mid	2.25	8	Changed flow rate
20	1000	4	Mid	1.75	7	Changed flow rate
21	500	4	Mid	0.75	5.5	Changed flow rate
22	3000	8	Mid	3.75	15	Changed standoff distance
23	2500	8	Mid	3.25	14	Changed flow rate
24	2000	8	Mid	2.75	13	Changed flow rate
25	1500	8	Mid	2.25	12	Changed flow rate

33

Test No	Flow Rate (SLPM)	Standoff Distance (ft)	North Station Flame Position	North Distance to Discharge Pipe (ft)	West Distance to Discharge Pipe (ft)	General Description / Additional Comments
26	1000	8	Mid	1.75	11	Changed flow rate
27	500	8	Mid	0.75	9.5	Changed flow rate
28	3000	~6.5	Scoping	7.5	11	Increased outlet from 1.5" to 3" dia.
29	3000	4	Tip	5	8.5	Adjusted to flame tip position
30	3000	~0	Scoping	7.5	11	Changed outlet size to ½-in dia.
31	3000	4	Tip	11.5	15	Adjusted to flame tip position
32	3000	4	Vertical	4	4	1.5-in diameter outlet
33	3000	4	Vertical	4	4	3-in. diameter outlet
34	Range**	4	Vertical	4	4	0.5-in diameter outlet

ND: Not Determined

*Flame was unstable at higher flow rates for this diameter discharge outlet. Testing started at 500 SLPM and ramped up to a maximum of 2000 SLPM.

Initial scoping tests were conducted to optimize the ignition procedure and standoff distances for heat flux and temperature measurement points. The position of the flame tip was determined visually, and this length was divided in half of the tests conducted with the instrumentation stations located at the midpoint of the flame length. The following specific parameters were evaluated:

- 500-3000 SLPM natural gas flow rate range

- 4-ft and 8-ft standoff distances from flame tip and flame middle

- Additional test runs with different diameter outlets

- Additional test runs with vertical discharge orientations

5.1.4 Test Results

Table 6 and Table 7 provide average summary results for the North and West measurement stations, respectively. Heat Flux (HF) data are shown in units of kW/m^2 and Thermocouple (TC) data are shown in units of °C.

Table 6. Summary of average test results for north measurement station

Test No	North Measurement Station (kW/m^2) & (°C)					
	1.5' HF	1.5' TC	4.5' HF	4.5' TC	7.5' HF	7.5' TC
2	10.1	174.5	15.7	182.4	12.4	177.7
3	9.5	191.3	12.9	192.1	10.5	192.9
4	7.4	168.1	10.9	157.7	9.8	161.1
5	7.9	174.2	12.2	181.8	9.9	169.4
6	6.4	134.1	9.6	147.5	7.5	135.4
7	5	131.7	7.5	153.6	5.6	128.3
8	3.9	98.8	4.6	102.9	2.6	76.7
9	3.8	92.8	5.2	94.5	5.5	96.2
10	4.2	112.8	5.6	110	5.5	108.4
11	3.5	99.1	4.4	103.6	4.6	101.9
12	2.8	86.4	3.3	89.9	3.5	89.9
13	1.8	77.1	2	76.7	2.2	76.8
14	0.9	51.1	0.8	53.7	1	51.8

Test No	North Measurement Station (kW/m²) & (°C)					
	1.5' HF	1.5' TC	4.5' HF	4.5' TC	7.5' HF	7.5' TC
15	11.9	164.7	16.2	197.3	9.8	155.6
17	11.7	156.7	14.2	199.1	6.5	139
18	9.5	139.6	12.2	183.5	6.9	141.4
19	7	141.5	9.9	165.1	6.5	135.1
20	4.4	119.1	6.1	127	4.6	105.5
21	3.6	110.5	4.1	116.2	2.4	83.7
22	5	98.6	5.9	110.3	4.9	97.3
23	4.8	85.7	5.7	112.5	4.9	106.8
24	3.7	74.4	4.1	94.2	3.7	93.3
25	2.9	75.2	3.3	92	3.1	87.6
26	1.9	68.4	2.1	80.5	2	74.2
27	1	58.2	0.9	60.9	1	57.4
28*	5.1	141.7	8.8	156.7	9.3	163
29	11	214.8	20.7	286.8	18.9	266.6
30*	8.3	112.3	6.5	105.2	3.1	77.2
31	4	135.3	4.7	114.3	2.8	71.6
32	1.9	74.2	4.7	125.3	7.7	141.4
33	2	79.4	5.1	137.7	9.2	163.6
34**	1.2	65.2	3.1	110.2	5.8	120.5

HF: Heat Flux
TC: Thermocouple
*Scoping runs to find correct standoff distance for different outlet diameters
**Values in table are for 2000 SLPM flow rate

Table 7. Summary of average test results for west measurement station

Test No	West Measurement Station					
	1.5' HF	1.5' TC	4.5' HF	4.5' TC	7.5' HF	7.5' TC
2	7.1	116.4	11	151.5	10.6	128.2
3	8.1	135.6	12	185.2	11.5	138.3
4	1.1	36.5	11.1	136.8	9.8	121.3
5	6.7	124.9	10.9	177.2	10.8	116.9
6	2.1	49.9	9.2	90.6	7.1	114.4
7	0.9	36.3	7.2	85	5.1	87.1
8	3.5	87.8	4.6	59.9	2	62.2
9	2.8	71	3.5	72.1	3.8	60.5
10	2.6	72.3	3.3	83.1	3.3	65.9
11	2.2	80.9	2.9	86	2.8	64.3
12	1.9	73.5	2.2	74.4	2.1	60.2
13	1.4	63.5	1.8	55.8	1.3	50.9
14	0.6	50.4	0.7	51.2	0.5	38.8
15	5.7	95.5	10.1	148.7	9.6	103.2
17	6.8	133.9	12	184.9	11.6	128.1
18	5.6	106.2	11	172.7	10.3	122.3
19	4.3	109.1	9	167.8	6.6	101.4
20	3.2	104.5	5.6	143.5	3.7	81.7
21	3.4	96	3.8	124.7	1.5	61.3
22	2.8	74.1	3.5	80.7	3.7	69.3
23	2.5	71.7	3.1	88.8	3.2	67.6
24	2.2	72.2	2.8	82.4	2.7	61.3

Test No	West Measurement Station					
	1.5' HF	1.5' TC	4.5' HF	4.5' TC	7.5' HF	7.5' TC
25	1.9	74.3	2.2	76.7	2	59.9
26	1.3	64.9	1.6	67.8	1.3	52.6
27	0.8	51.7	0.9	58.7	0.6	45.2
28*	4.1	91.2	6.1	112.3	7.9	94.1
29	6.8	137	15.9	149.6	17.9	173
30*	16.8	186.2	43.5	514.2	27	436.9
31	3	71.3	3.5	100.7	8.2	225.8
32	1.7	50.5	3.8	83.4	7.2	97.8
33	1.8	54.3	4	87.4	7.6	101.5
34**	1.1	45.1	2.7	73.4	5.1	86

HF: Heat Flux

TC: Thermocouple

*Scoping runs to find correct standoff distance for different outlet diameters

**Values in table are for 2000 SLPM flow rate

Figure 37 and Figure 38 provide plots of the time history of heat flux and thermocouple (i.e., temperature) measurements, respectively, from Test 15 (3000 SLPM, 4-ft Standoff Distance, Flame Middle). Figure 39 and Figure 40 provide similar charts but for Test 22 (3000 SLPM, 8 -ft Standoff Distance and Flame Middle Location). The temperature data provided in Table 6 and Table 7 were averaged over the last 30 seconds of the test (2-2.5 min), but for average heat flux data, these values were averaged between the final 60 to 120 s, since these values came to steady state much faster than the temperatures. This general approach was taken for all averaging calculations.
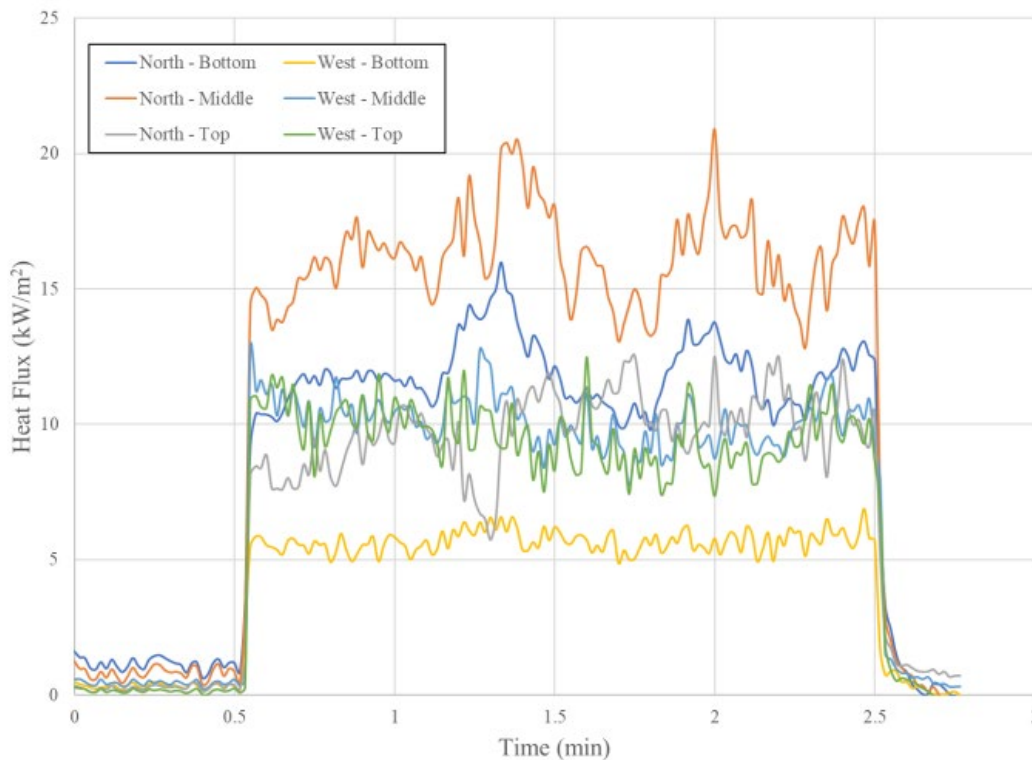

Figure 37. Heat flux time history for Test 15 (3000 SLPM, 4-ft standoff distance and flame middle location)
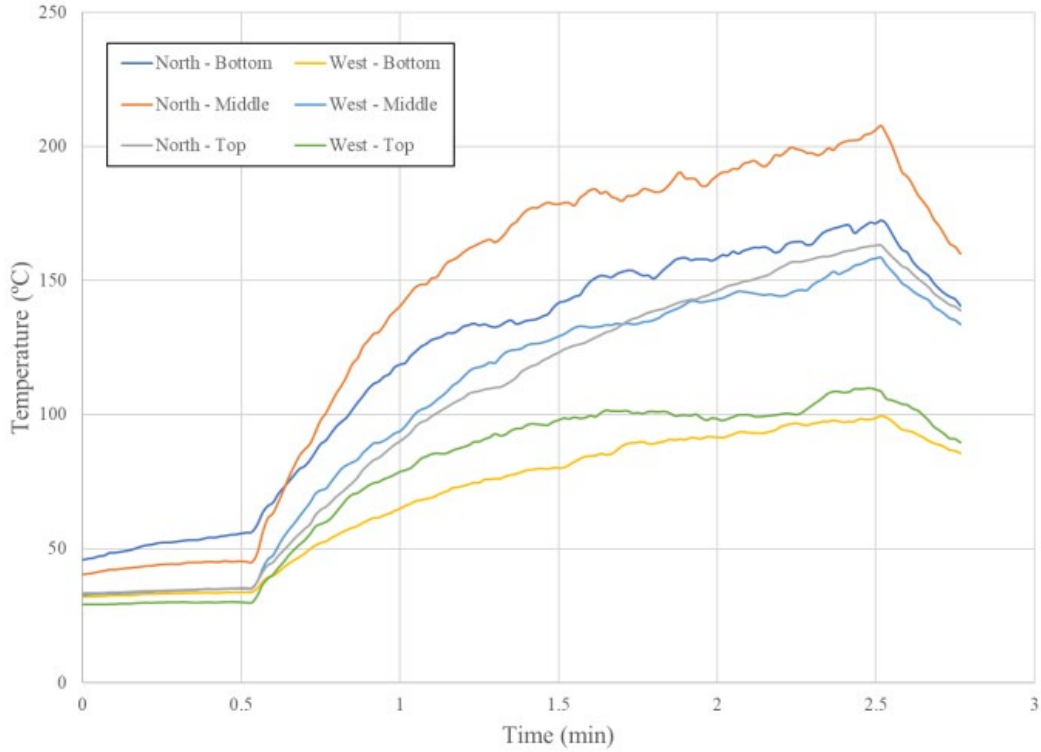
Figure 38. Temperature time history for Test 15 (3000 SLPM, 4-ft standoff distance and flame middle location)
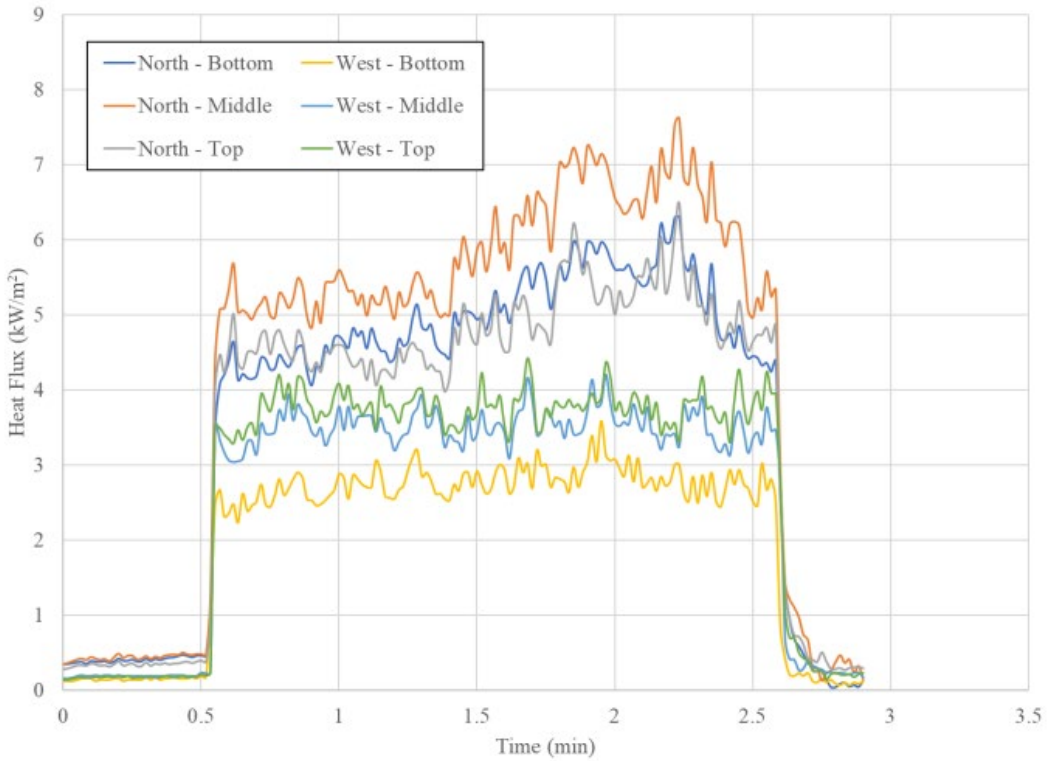

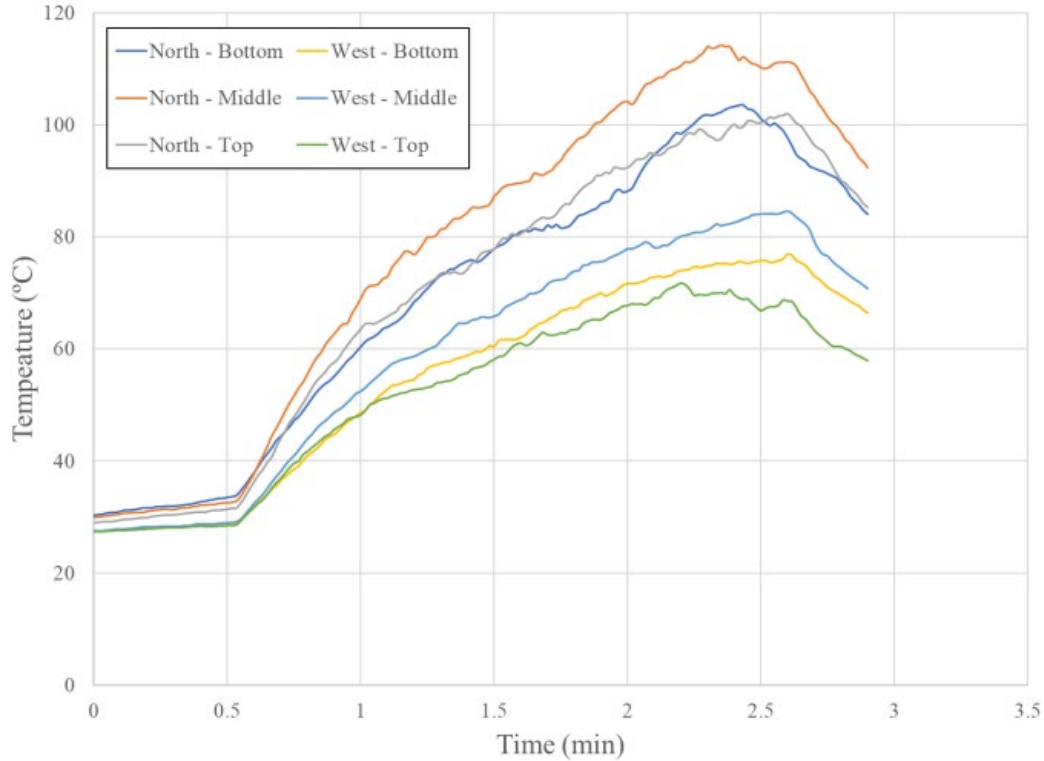**Figure 39. Heat flux time history for Test 22 (3000 SLPM, 8 -ft standoff distance and flame middle location)**

37

Figure 40. Temperature time history for Test 22 (3000 SLPM, 8 -ft standoff distance and flame middle location)

5.1.5 Discussion

Figure 41 provides a summary of the average heat flux data collected at a 4-ft standoff distance from the flame tip as a function of natural gas flow rate. Figure 42 provides a similar chart but at the flame middle position.

The overall trend of increasing heat flux with increasing flow rate was observed for both series of tests. It can also be seen that the 1.5-ft height measurement points seem to have the most variation followed by the 7.5-ft height location. The most consistent trend was observed for the 4.5-ft height which is likely due to the measurement point seeing the highest consistent percentage of flame during testing. Peak heat fluxes are slightly higher for the Flame Middle measurement position compared to the flame tip position which is likely due to the more intermittent exposure close to the flame tip as compared to the middle.

Figure 43 and Figure 44 show similar comparative graphs for the 8-ft standoff distance. As expected, lower heat fluxes were observed compared to the 4-ft standoff distance. The heat fluxes measured at the 1.5-ft elevation were again the lowest as compared to the other heights; however, the increasing trend with increasing flow rate was more consistent for the 8-ft standoff distance compared to the 4-ft standoff distance. Again, this is likely due to a more even distribution of heat and less turbulence effect at the 8-ft distance compared to the 4-ft distance.

Figure 41. Heat flux trend for 4-ft standoff distance and flame tip location

Figure 42. Heat flux trend for 4-ft standoff distance and flame middle location
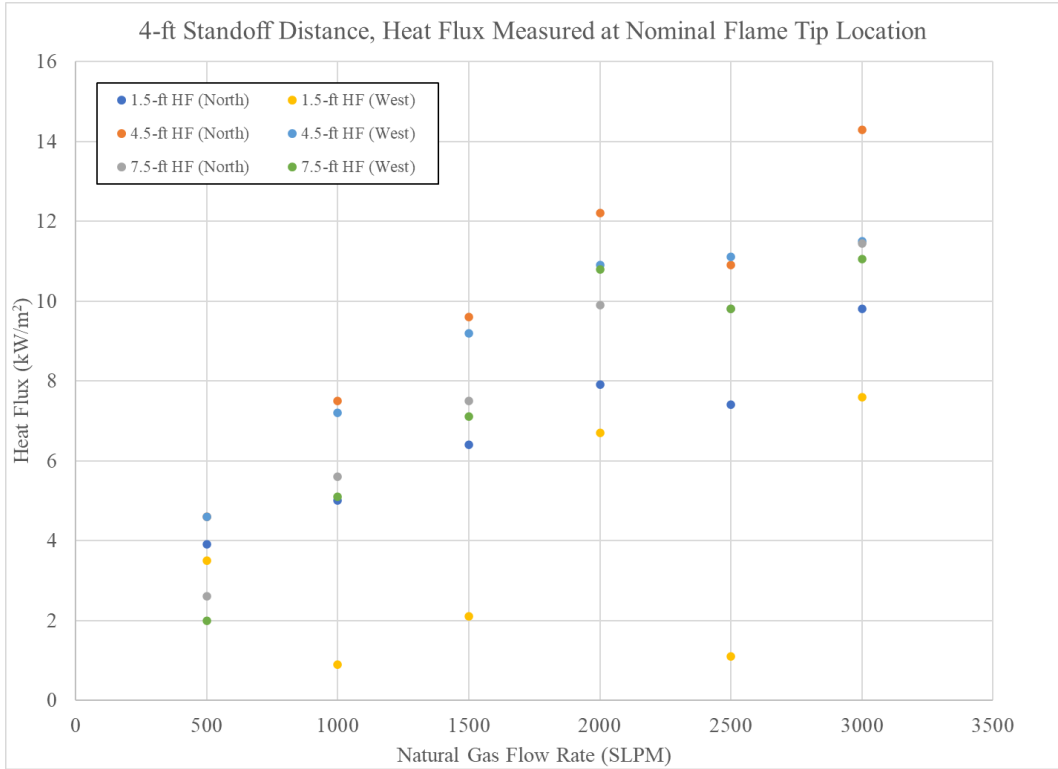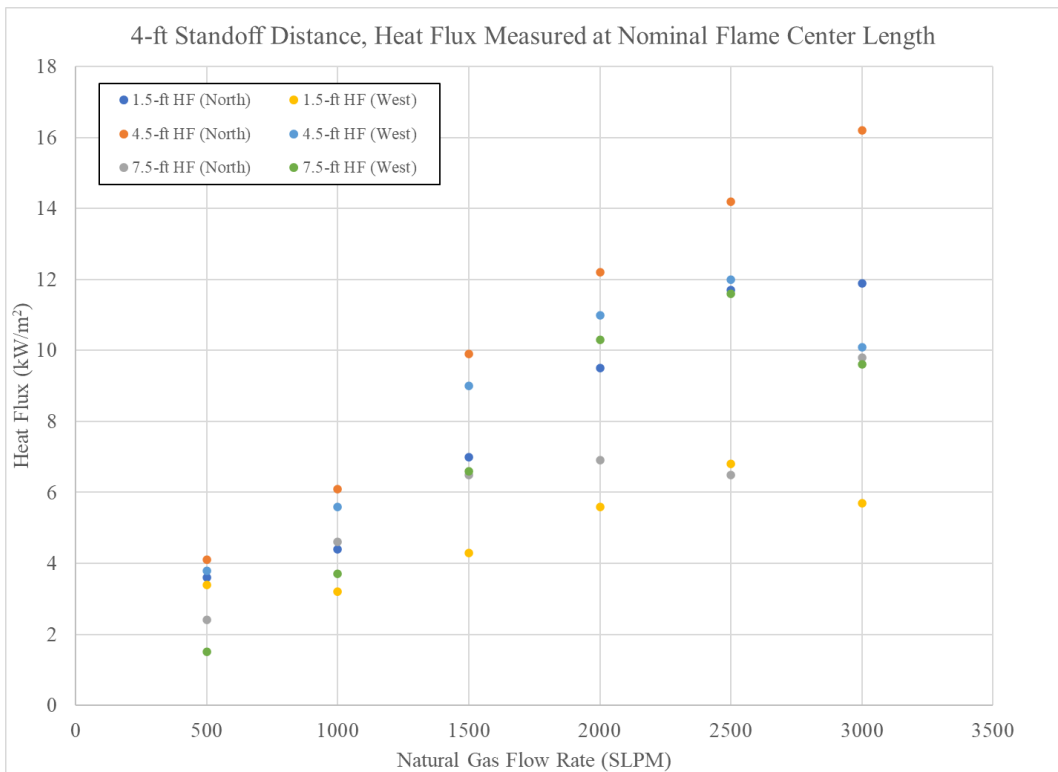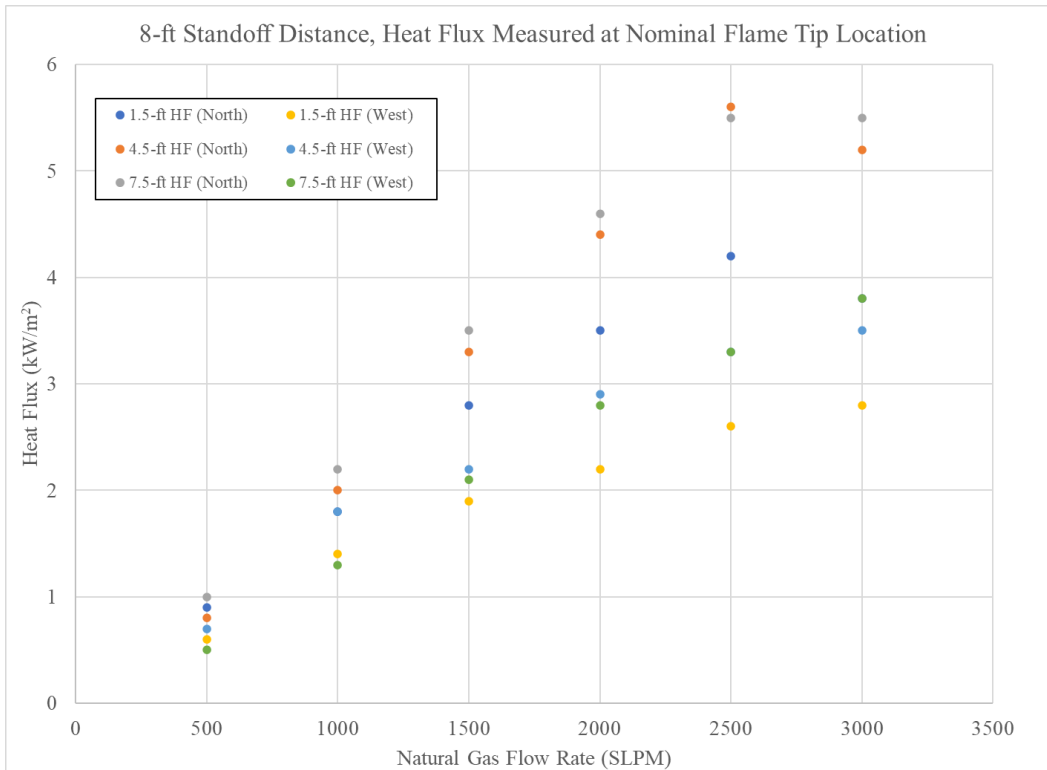
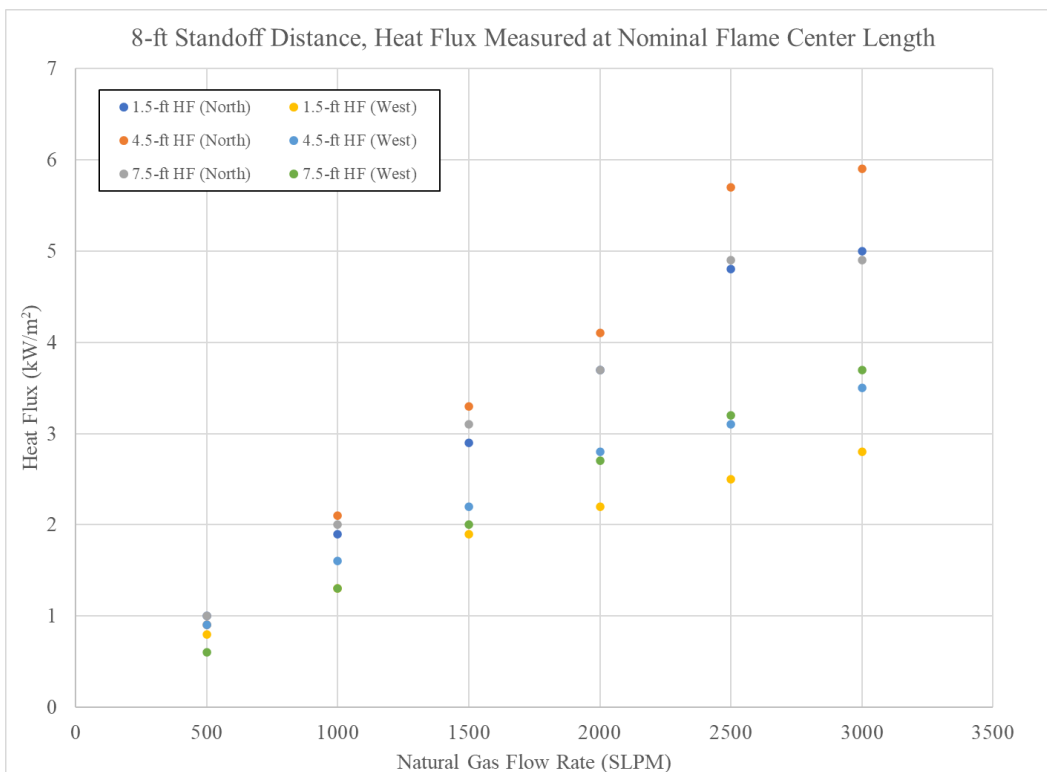**Figure 43. Heat flux trend for 8-ft standoff distance and flame tip location**

Figure 44. Heat flux trend for 8-ft standoff distance and flame middle location

Figure 45 shows a comparison between peak heat fluxes measured for each flow rate and each configuration. For the 4-ft standoff distance, the peak heat flux varies from 4-16 kW/m^2 across the flow rate range. For the 8-ft standoff distance, the heat flux range is 1-6 kW/m^2.
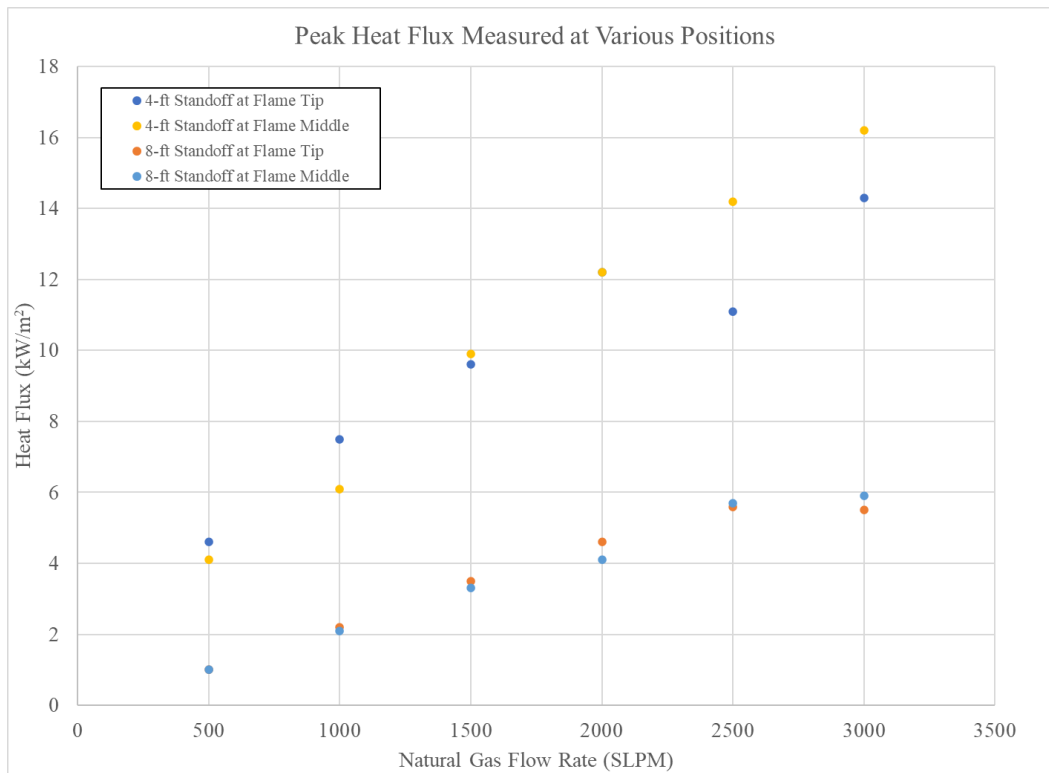
Figure 45. Peak heat flux comparative chart

At a 4-ft standoff distance from the flame all flow rates (500+ SLPM) generated incident heat flux that exceeded the capabilities (~1 kW/m^2) of standard personal protective equipment (PPE) (Heus & Denhartog, 2017). For the 4-ft standoff distance incident heat flux at flow rates of 1000+ SLPM exceeded the 3-min working time for firefighter PPE (4.6 kW/m^2) and at flow rates of 1500+ SLMP exceeded the 5-min working time for aluminized PPE (6.3 kW/m^2).

At 8-ft standoff, flow rates of 1000+ SLPM created heat flux that exceeded the ability of industry standard PPE to protect personnel for an extended period. Firefighter PPE could withstand the heat flux generated at 8 ft for flow rates of 2000 SLPM and below for at least 3 min. The capabilities of aluminized PPE are expected to provide sufficient protection at an 8-ft standoff distance for flow rates up to 3000 SLPM.

For reference, the predicted total leak rate through closed fire damaged PRVs and other fire damaged valves is 6000 – 12,000 SLPM (FRA, 2023). Note that there are up to 20 valves in addition to the PRV(s) located in the piping cabinet, depending on the tank design, which are almost certain to fail after 10-20 minutes of fire exposure. Thus, the heat flux generated just from ignited natural gas leaking from valves could easily exceed the protective capabilities of emergency personnel PPE within an 8-ft radius.

6. Structural Countermeasures

The structural FE model was used to evaluate select design features that could improve the crashworthiness of a UN-T75 tank by protecting the PRV piping assembly. Damage to piping that can restrict PRV flow was shown to occur at impact speeds as low at 10 mph (see Section 3). The countermeasures evaluated were limited to structural features that would protect the PRV system in its existing position. Changes in the layout of the PRV piping could provide additional benefits.

6.1 Methodology

The UN-T75 tank FE model was modified to include additional structural members that would protect the PRV system from damage in derailment crash conditions. Ad hoc simulations were conducted to evaluate custom structural improvements that, based on engineering judgement, were likely to reduce the amount of damage sustained by the PRV assembly in two crash configurations: end-on impacts to the piping cabinet with a flat car and perpendicular impacts to the top end with a rigid pole. The rollover cases were not investigated due to the low risk of generating direct damage to the PRV piping assembly.

Structural components were created in FE and added to the existing model. The crash conditions remained the same as described in Section 3. Two countermeasures were considered that represented modifications that could reasonably be added without considerably affecting the cost or weight of the tank system. A "crash cushion" style countermeasure (Figure 46) was created out of 4 x 6 x 1/4 inch square tubing using the same material properties as the tank's existing frame structure. This assembly added 426 kg (939 lb) to the tank, which represents about 3.5 percent of the tank's empty weight. The second countermeasure involved increasing the wall thickness of the PRV piping assembly from 0.154 inch to 0.25 or 0.5 inch.
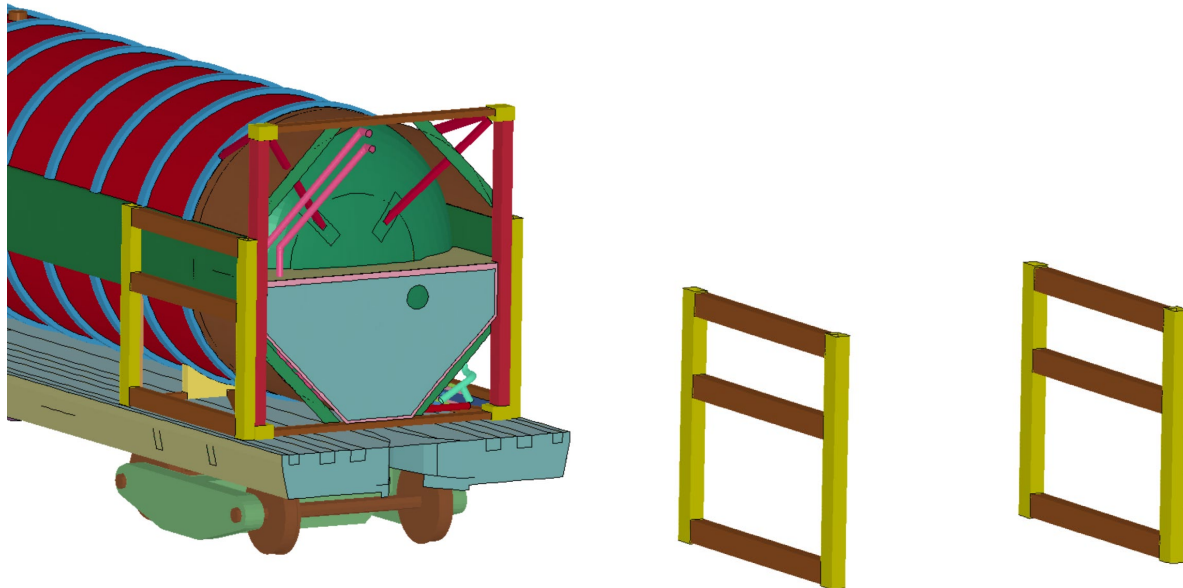
Figure 46. "Crash Cushion" Countermeasure

6.2 Results

The "crash cushion" countermeasure was able to completely prevent pipe damage in a 15-mph end-on impact with a flat car. At 20 mph (1.78 times more energy) the pipe damage with the countermeasure was similar to the baseline case at 15 mph.
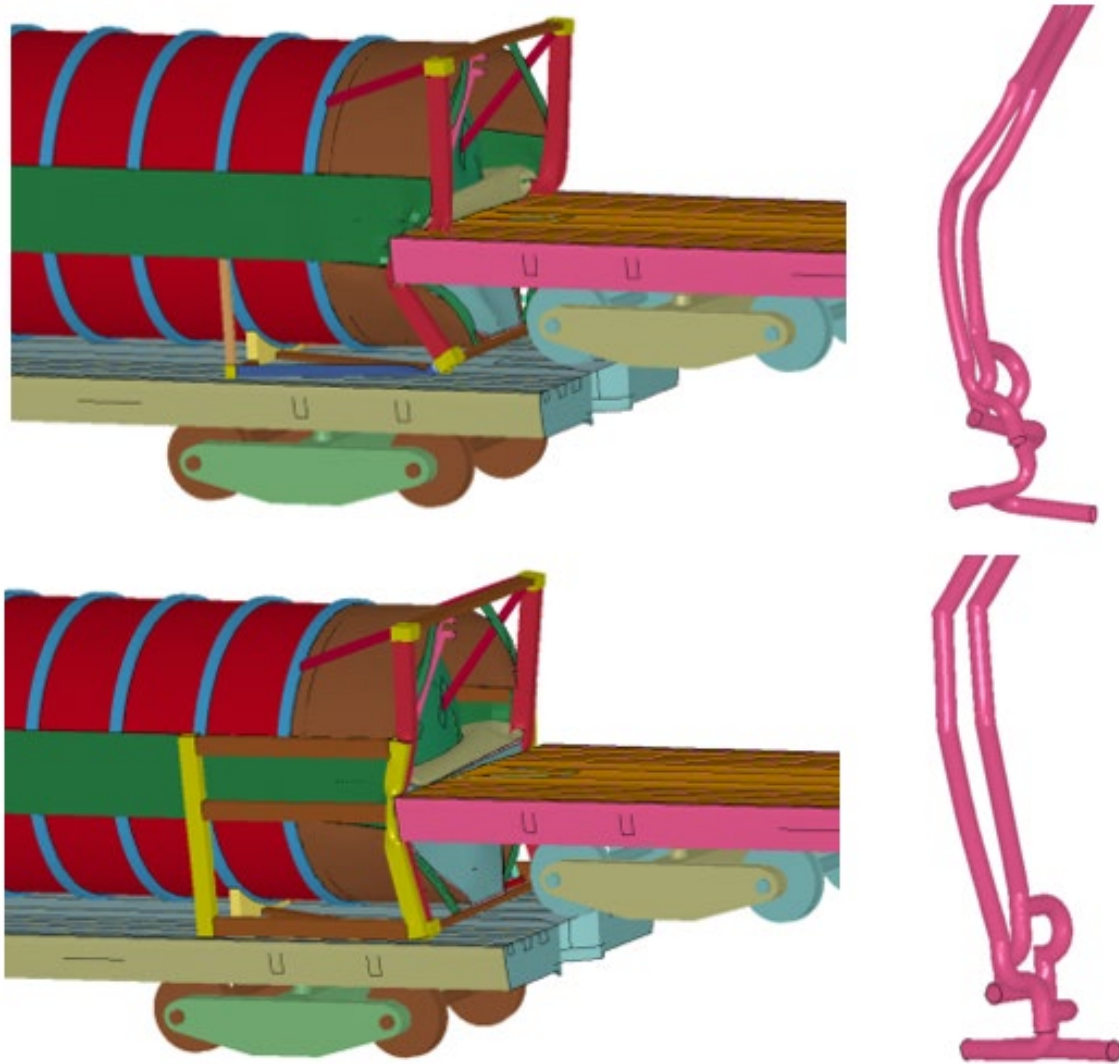
Figure 47. Maximum damage in 15 mph rear impact for baseline tank (top) and countermeasure (bottom)
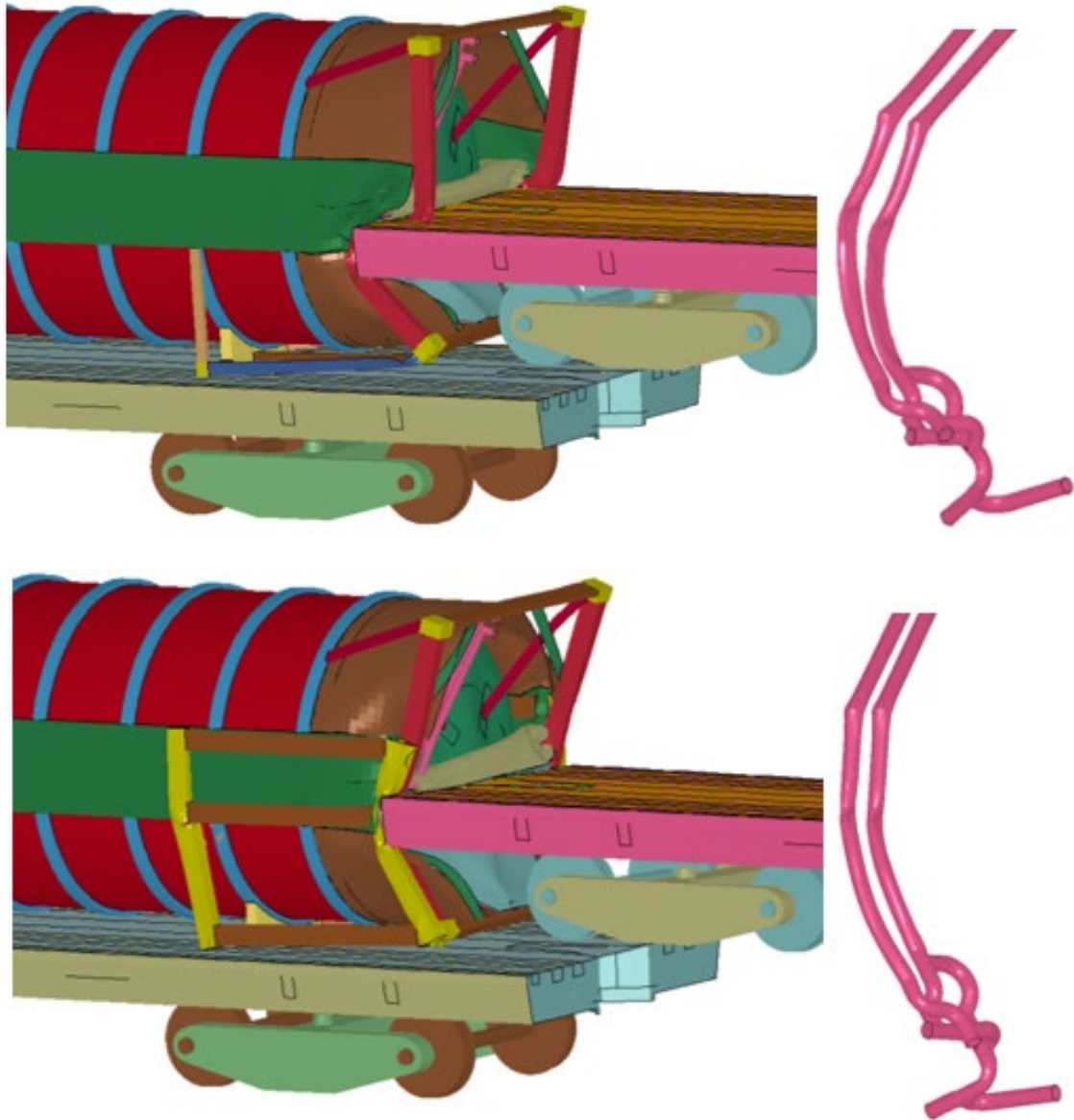
Figure 48. Maximum damage in 20 mph rear impact for baseline tank (top) and countermeasure (bottom)

The thickened pipe countermeasures proved to be very effective in mitigating crush damage to the pipe (Figure 49). At 30 mph the baseline pipe was completely pinched closed, the 0.25-inch thick pipes were >95 percent closed, and the 0.5-inch-thick pipes were 25 percent closed (Figure 50). Similar results were observed for the internal pipes.
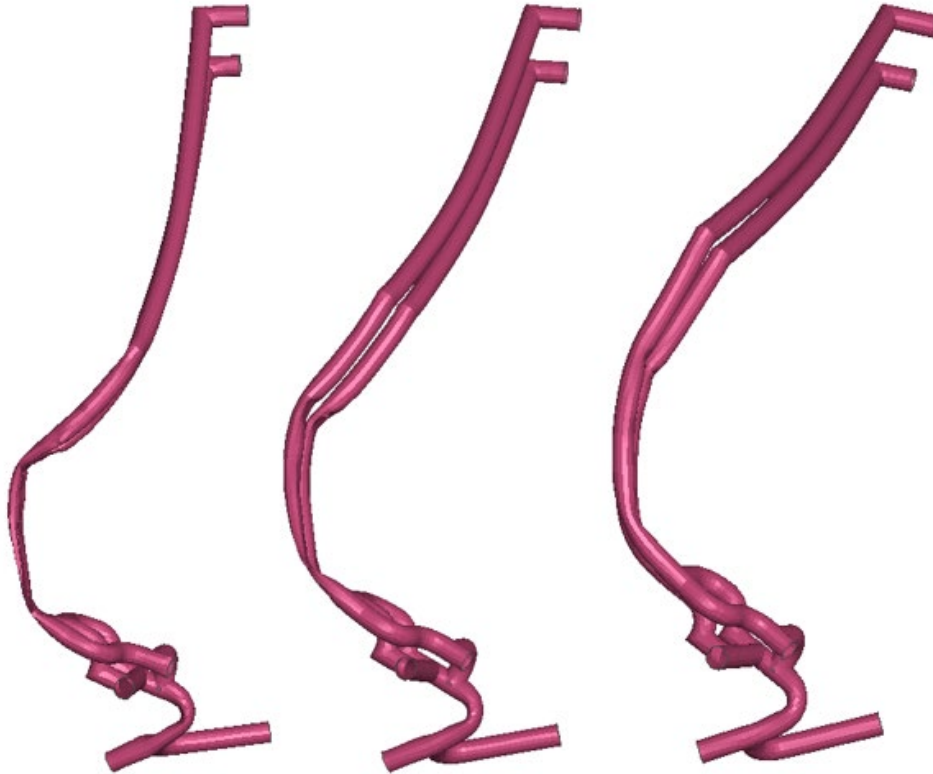
Figure 49. External PRV Piping Assembly after 30 mph impact with empty flatcar: Baseline Sch 40 pipe (left); 0.25" thick pipe (center); 0.5" thick pipe (right)
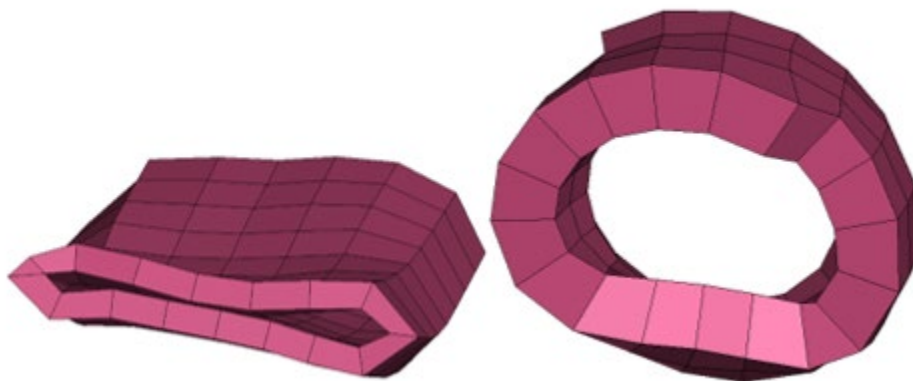
Figure 50. Maximum deformation of 0.25" (left) and 0.5" (right) thick external PRV pipes

7. PRV Exhaust Flame Effects

Ignition of the PRV exhaust is highly likely for flammable fluids when exposed to nearby fire such as a pool fire. Due to the moderate mass flow rate through the PRV system under nominal conditions and the high mass flow rate through the PRV system under overturn/dual-phase conditions (see Section 4), the resulting jet flame can provide a significant heat load to neighboring tanks.

7.1 Methodology

Fire Dynamics Simulation software (FDS, NIST) was used to simulate the subject UN-T75 tank and fire conditions. The 3-dimensional tank model included the external tank geometry and a representation of a flat car on which it was positioned (Figure 51). The steel materials were modeled with appropriate thermal properties.

Figure 51. Tank and Flat Car Model within the FDS environment
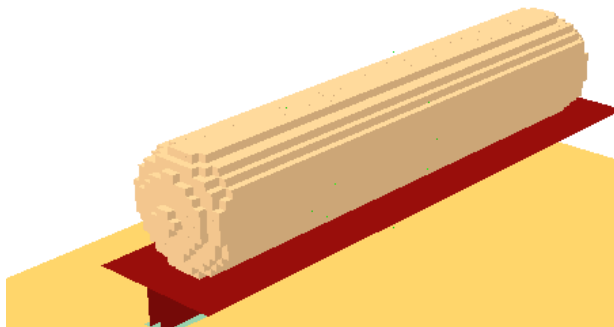
Combinations of two fire loads were applied to the tank/flat car model: a pool fire and a jet flame. The pool fire was meant to represent the same size and heat release rate as the fire used in the FRA fire tests (Friedman & Mattos, 2018; FRA, 2023). The output data of interest for each of the models was the total net steady-state heating to the tank (discussed in the Results section).

The pool fire was 40 ft x 13 ft (12.19 m x 3.96 m) and provided a heat release rate per unit area (HRRPUA) of either 4564 kW/m^2 (High) or 2282 kW/m^2 (Low). The pool fire was modeled as a propane-fed area with a mass flow rate defined to achieve the desired HRRPUA. For reference, the target HRRPUA of the FRA fire tests was 4564 kW/m^2.

The jet fire model was meant to replicate the highest (500 lb/min) and lowest (150 lb/min) mass flow conditions determined through physical testing in this project (see Section 4). The jet fire was either directed at the end of the tank and parallel with its axis (i.e., END) or perpendicular to the center of the tank (i.e., SIDE). The jet fire was positioned either 1.1 m (i.e., CLOSE; minimum nominal distance between neighboring flat cars), 6.1 m (i.e., MID), or 11.1 m (i.e., FAR) from the tank. In each case the jet was positioned 0.1 m above the ground to mimic its position on an overturned tank (see Figure 52 for a view of the model setup). The exhaust jet was composed of "cryogenic" liquid methane droplets defined with a set of parameters (i.e., spray angle, evaporation rate, particle size, and initial velocity) that were calibrated against large-scale, high-pressure jet fire test data (Lowesmith & Hankinson, 2012). The thermal properties of the droplets and resulting gas were defined by the NIST-provided library within the FDS solver.
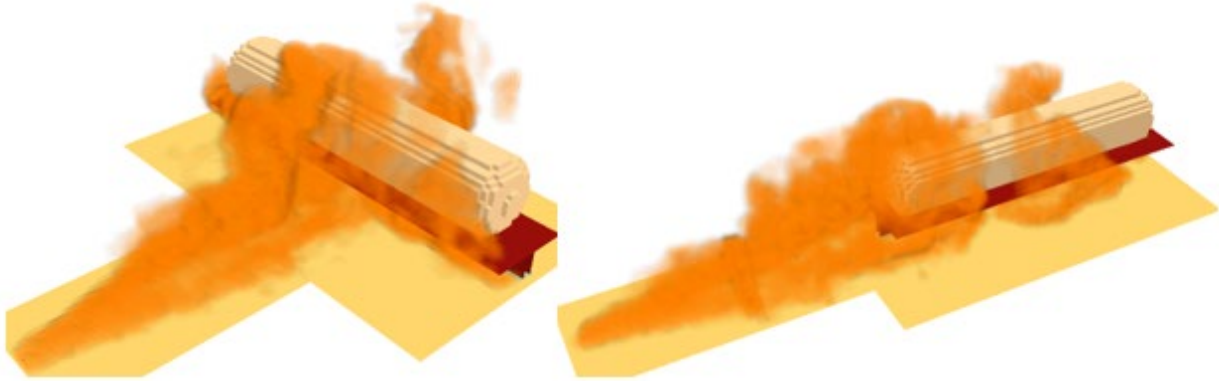
Figure 52. Example visualizations of the FAR jet fire position in the SIDE (left) and END (right) configurations without a pool fire

The matrix of 28 simulation conditions is summarized in Table 8.

Table 8. Fire Impingement Simulation Matrix

Pool Fire HRRPUA	Jet Fire Mass Flow Rate	Jet Direction	Jet Distance
LOW	HIGH	END	CLOSE
LOW	LOW	END	CLOSE
-	HIGH	END	CLOSE
-	LOW	END	CLOSE
LOW	HIGH	SIDE	CLOSE
LOW	LOW	SIDE	CLOSE
HIGH	HIGH	SIDE	CLOSE
HIGH	LOW	SIDE	CLOSE
No	HIGH	SIDE	CLOSE
No	LOW	SIDE	CLOSE
LOW	HIGH	END	FAR
LOW	LOW	END	FAR
HIGH	HIGH	END	FAR
HIGH	LOW	END	FAR
No	HIGH	END	FAR
No	LOW	END	FAR
LOW	HIGH	SIDE	FAR
LOW	LOW	SIDE	FAR
-	HIGH	SIDE	FAR
-	LOW	SIDE	FAR
LOW	HIGH	END	MID
-	HIGH	END	MID
-	LOW	END	MID
LOW	HIGH	SIDE	MID
-	HIGH	SIDE	MID
-	LOW	SIDE	MID
BASELINE			
LOW	-	-	-
HIGH	-	-	-

Pool fire HRRPUA: LOW = 2282 kW/m^2; HIGH = 4654 kW/m^2
Jet Fire Mass Flow Rate: LOW = 1.134 kg/s; HIGH = 3.74 kg/s

7.2 Results

In the baseline (pool fire only) simulations the steady-state heating rate across the entire tank was 4120 kW for the LOW case and 5100 kW for the HIGH case. The addition of a jet fire had mixed results in terms of altering the total heating rate of the tank, which can be seen in Figure 53.
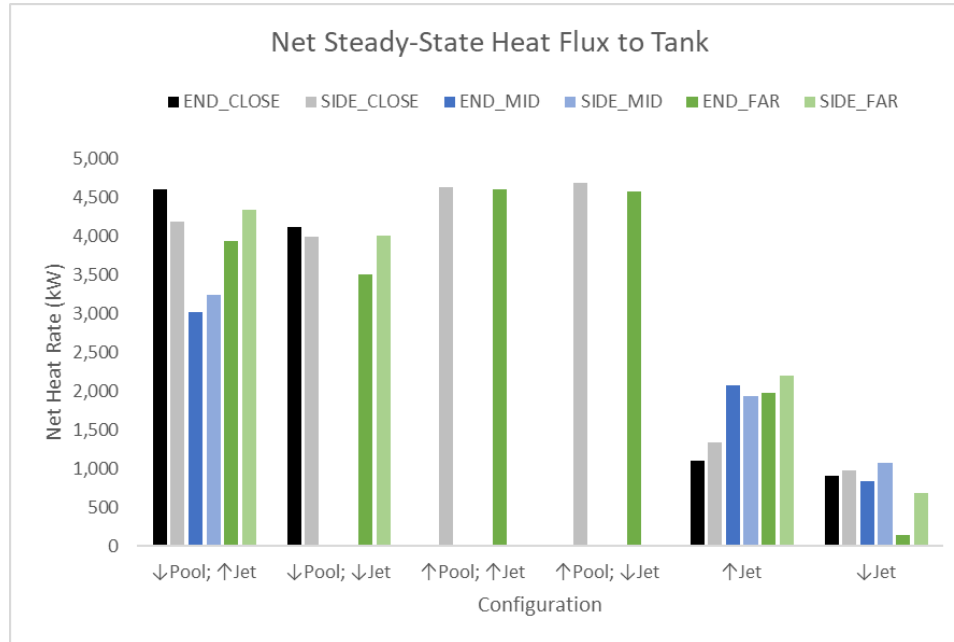
Up arrow represents the "HIGH" condition and down arrow represents the "LOW" condition

Figure 53. Summary of heating rates for the simulated fire conditions

In the LOW pool fire conditions, the addition of the HIGH jet flame marginally increased the overall heating rate for some conditions (END_CLOSE, SIDE_CLOSE, SIDE_FAR) while it decreased the heating rate in others (END_MID, SIDE_MID, END_FAR). For the combined LOW pool fire and LOW jet fire condition all heating rates were equal to or lower than the LOW pool fire only condition.

For the HIGH pool fire condition, all the jet fire configurations resulted in a lower heating rate than the baseline case.

In the jet fire only conditions, the heating rate for most of the HIGH jet conditions was roughly half that of the pool fire conditions. The LOW jet fire only cases resulted in heating rates approximately 25 percent of the pool fire only cases. The HIGH jet configurations always produced greater heating than the LOW jet configuration. In the HIGH jet fire only configurations the 1 m standoff distance produced less heating than the 6.1 and 11.1 m distances.

The jet flame increased the heating on the tank where it directly impinged on it. An example of this is demonstrated by comparing Figure 54 and Figure 55. The pool fire alone did not appreciably apply direct heat to the tank ends; however, the jet fire directed at the end of the tank resulted in an average incident heat flux of approximately 60-100 kW/m^2 and peaking at ~125 kW/ m^2. Some of the peak heating rates appeared to be offset by the cooling effect of the cryogenic liquid methane drops that moved along with the momentum-driven flow.
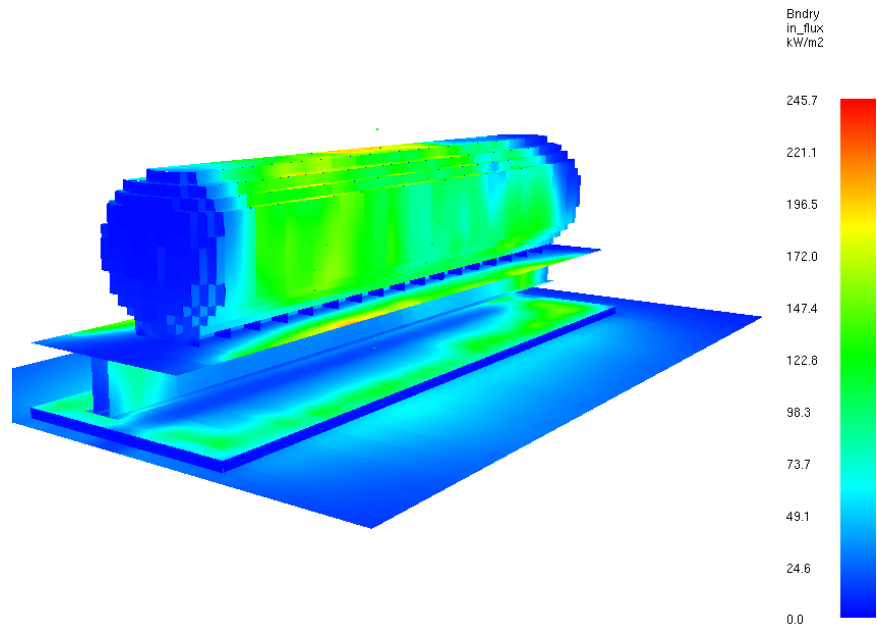
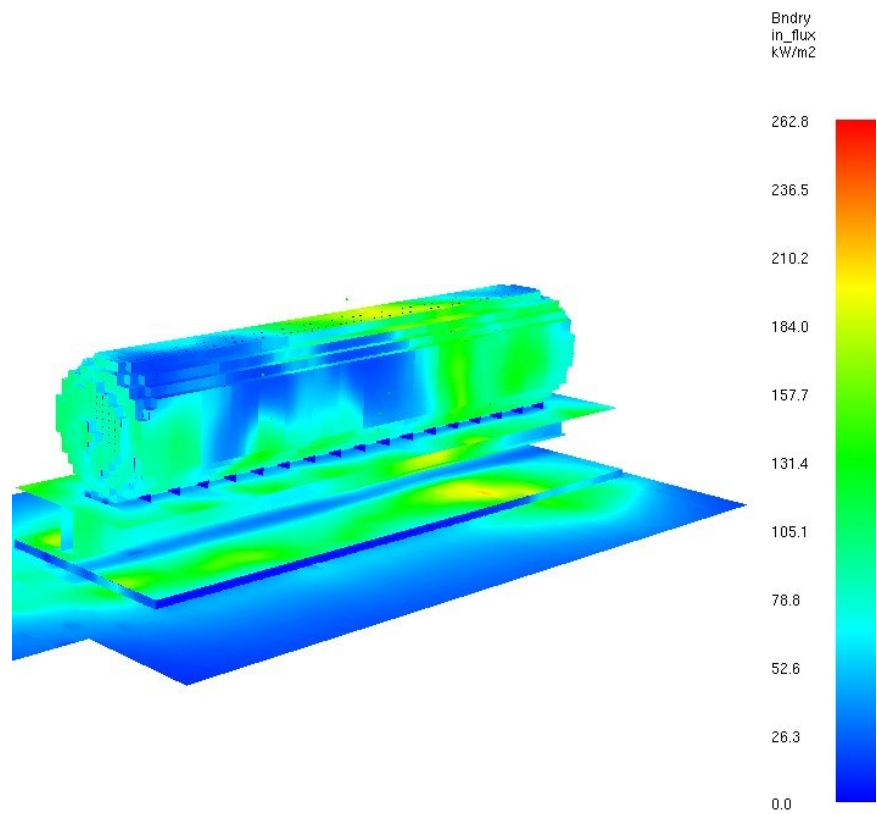**Figure 54. Incident heat flux on tank exterior in the HIGH pool fire only configuration**

Figure 55. Incident heat flux on tank exterior in the HIGH pool fire + HIGH jet fire END configuration

7.3 Discussion

It is not surprising that the magnitude of total tank heating rate was relatively unchanged in the combined pool fire + jet fire cases. The size of the pool fire itself is sufficient to considerably affect the amount of available oxygen around the tank. The additional fuel provided by the natural gas jet resulted in a fuel-rich condition with more fuel available than could be burned. This is also exemplified in the marginal heating rate increase between the two LOW and HIGH Baseline conditions in which the fuel rate was doubled but the heating rate only increased by 24 percent. This effect can be visualized by the oxygen molar fraction shown along the centerline of the model in Figure 56 and Figure 57. Additionally, the strong flow of liquid and gas in the exhaust jet resulted in an effective 'wind' on the order of 3 to 5 m/s around the tank and up to 30 m/s below the railcar. The combination of the added jet flame, the richness in the fuel mixture, and the added 'wind' effectively cancelled out any added heating by the jet itself.
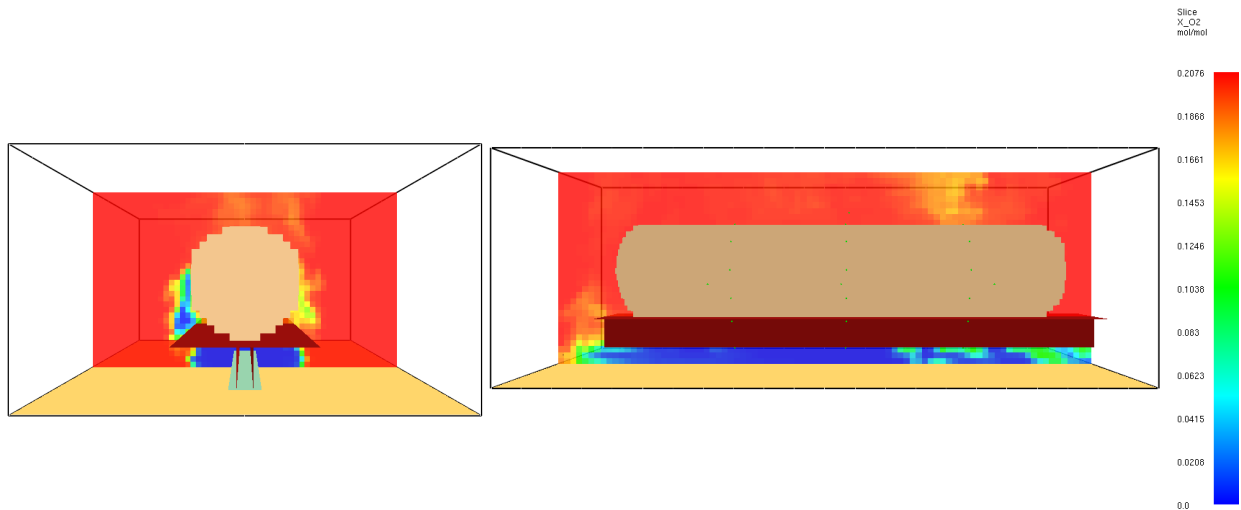

Figure 56. Molar fraction of oxygen in a LOW, END, CLOSE, Jet configuration (no pool fire)
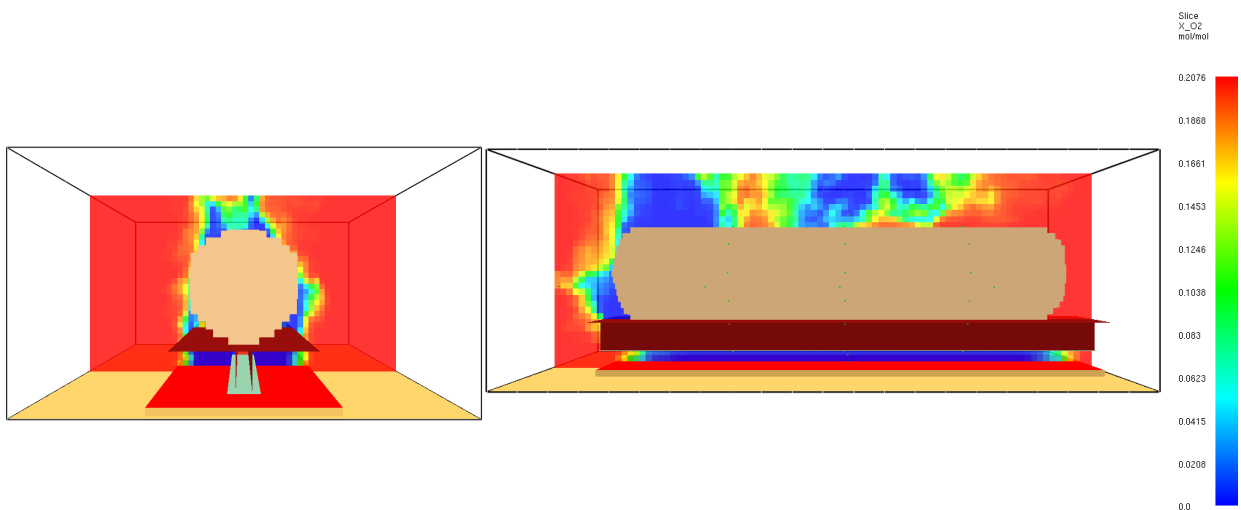

Figure 57. Molar fraction of oxygen in a LOW, END, CLOSE, Jet configuration (LOW pool fire)

The localized heating from the jet flames in this study (peak = ~125 kW/m^2) was substantially less than what was observed from similar simulations of jet flames formed from single (gas) phase flow of methane out of the PRVs at the nominal flow rates (peak = 178-292 kW/m^2) (Mattos & Friedman, 2023). These differences in peak incident heat flux can be explained by the differences in the test conditions. This study simulated the flow of cryogenic liquid methane out of a 50 mm pipe orifice at ground level between 1.1 and 11.1 meters from the target tank. The previous study simulated the flow of pure methane gas out of a 50 mm pipe at 0.5 m above the tank centerline between 1 and 5 m from the target tank. Both the location of the jet flame relative to the target tank and the use of cryogenic liquid, which was used to represent the dual phase flow observed in the test, likely resulted in the relatively lower incident heating rates. Nonetheless, the heat flux provided by the jet flame would be sufficient to thermally fail the seals in all the valves of the piping cabinet, included any PRVs, within 10 minutes of exposure or less.

8. Suggested Future Work

The results of the current and previous studies have highlighted knowledge gaps and areas for future work. Suggestions for future work are summarized below.

- Use multiphysics modeling to evaluate the crashworthiness and fireworthiness of tanks transported within well-cars. Well-cars typically have an open bottom, which may increase the thermal load applied from a pool fire compared to tanks transported on flat cars. Additionally, the raised walls of a well-car pose a potential impact surface that may directly damage external piping or the tank itself.

- Use the jet fire test data in this study to create validated FDS models.

- Extend the physical jet fire testing demonstrated in this report to higher flow rates, including dual-phase flows.

- Characterize the jet flame impingement on a cryogenic tank and/or external valves/piping. Localized heating from a jet fire is likely to degrade valves, the external tank, and annular space insulation much more quickly and severely than a pool fire.

- Evaluate the effects of non-methane components (e.g., ethane, toluene, benzene, etc.) within the LNG mixture during heating and PRV exhaust.

- Conduct full-scale or component-level physical testing to demonstrate countermeasures for protecting the PRV piping assembly from damage in a derailment condition.

9. Conclusion

The literature review, physical testing, and physics-based simulations conducted in this project provided novel data and insight into the thermal performance of cryogenic tanks subjected to fire conditions. The findings are summarized below.

- PRVs that meet the regulatory requirements for UN portable tanks and are typical of devices found on UN-T75 style tanks, while not specifically designed to exhaust dual-phase cryogenic fluid, were subjected to dual-phase flow of cryogenic liquid nitrogen at pressures ranging from 130 to 180 psi. Time histories of PRV temperature, mass flow rate, fluid density, and fluid pressure were recorded. Testing was very repeatable.

- At tank pressures in the range of those expected to exist in fire-exposed conditions, the dual phase mass flow rate through the PRVs was similar to the measured flow rates of high pressure (870 psi) natural gas through a 20 mm diameter orifice in the literature.

- The tested PRVs were found to provide flow rates that exceeded those required to maintain a safe working pressure under fire exposure when tested with liquid nitrogen in short duration tests. The dual-phase mass flow rate of liquid nitrogen through the PRVs was measured to be between 1.134 kg/s and 3.74 kg/s between tank pressures of 130 and 180 psi. This is 2.8 to 9.4 times greater than the single (gas) phase flow rate for the same PRVs. The dual-phase mass loss rate measured in this study is similar to the mass loss rate of natural gas through a 20 mm orifice in an 856 psi natural gas pipeline (~2.9 kg/s).

- A constriction representing 90 percent closure of the discharge pipe reduced the dual-phase mass flow rate out of the PRV by approximately 38 percent. The constriction also produced an oscillation in the flow which, if allowed to continue, could damage the PRV seal, springs, or other components through fluttering.

- The dual-phase PRV exhaust plume extended from 60 to 100 ft in length, and ignition of this plume could provide considerable heating to nearby tanks.

- All jet fire conditions evaluated in the study present a significant threat to emergency responders.

- A significant increase in flow rate was observed for the liquid nitrogen in the subcooled condition. This means that a freshly filled LNG tank would likely empty faster than a tank that has had time to heat up during its travel.

- The risk of a PRV "icing up" resulting from ambient moisture in humid conditions encountering the cryogenic piping assembly is predicted to be negligible when a sufficient length of pipe is attached to the PRV outlet.

- Natural gas jet fires were characterized across a range of low mass flow rates, orifice sizes, and orientations. These data can be used in the future to validate simulations of fire behavior and may be applied to tanks.

- Two simple structural countermeasures were demonstrated that could reduce the likelihood of PRV assembly damage and the associated risk of reduced mass loss rate. In some scenarios these countermeasures increased the damage-inducing speed from 10 mph to over 30 mph.
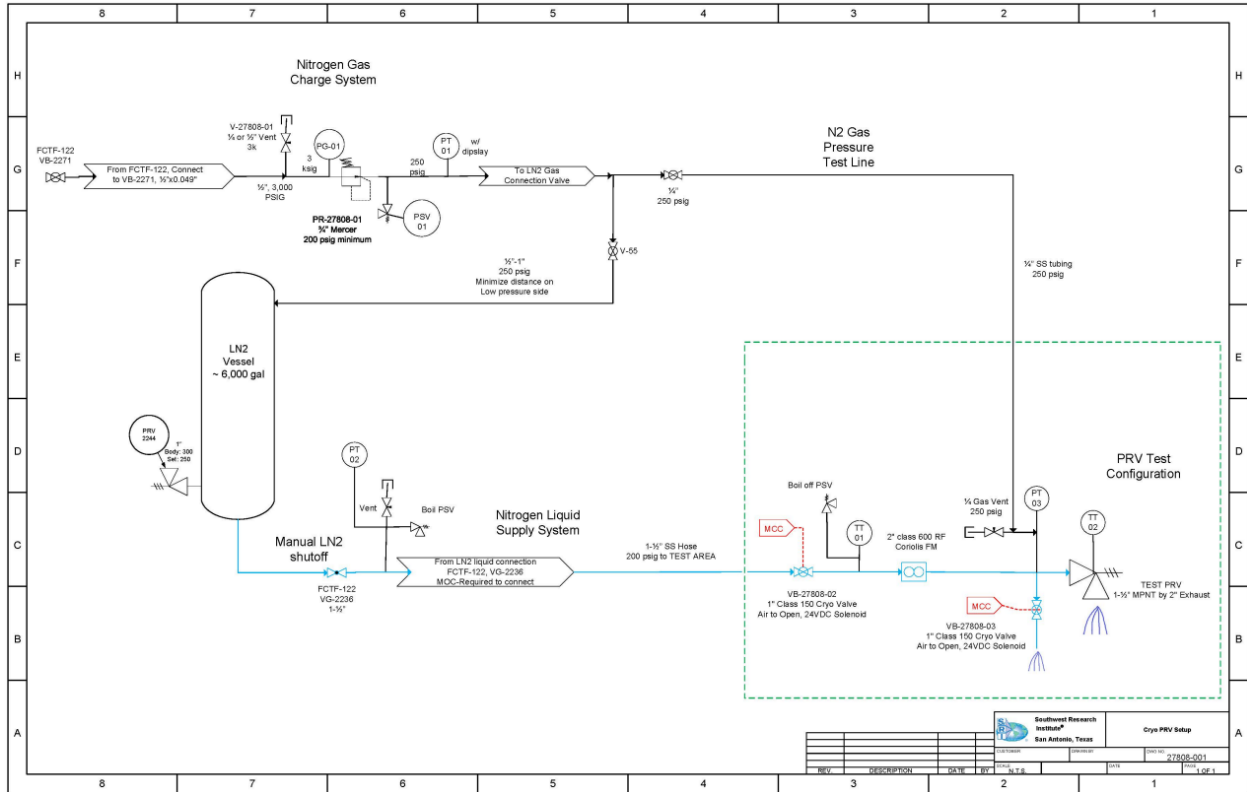
- Derailment and/or overturning of a cryogenic tank can result in the PRV assembly no longer meeting the performance requirements described in the regulations (49 CFR 178.274). These include restricted downstream flow, PRV inlet in the liquid space rather than the vapor space, and escaping vapor directed at the tank shell or neighboring tank shell. The impact of fire will likely prevent the PRV from closing after the pressure returns to below the set pressure.

10. References

Baker Hughes (n.d.). Consolidated 1900/1900 DM Series.

Federal Railroad Administration (2023). Fire Test of An UN-T75 Portable Tank on A Flat Car-Phase II (Report No. RR 23-01).

Friedman, K., & Mattos, G. (2018). Analysis of Liquid Nitrogen Test Data, Transport Canada, T8080-170208.

Heus, R. & Denhartog, E. (2017). Maximum allowable exposure to different heat radiation levels in three types of heat protective clothing. *Indus. Health, 55*, 529-536.

Lowesmith, B., & Hankinson, G. (2012). Large scale high pressure jet fires involving natural gas and natural gas/hydrogen mixtures. *Process Safety and Environmental Protection, 90*, 108-120.

Mattos, G. & Friedman, K. (2023). Final Report: Modelling of ISO [UN-T75] Portable Tank Fire Test, Transportation of Dangerous Goods. Transport Canada.

Prabhakaran, A., et al. (2022). Performance of Tank Car Pressure Relief Devices Under Derailment Fire Conditions (Report No. DTFR53-17-C-00015).

Rockwood Swendeman (n.d.). Bronze Safety Relief Valves, Type RXSO. Circle Cryogenics.

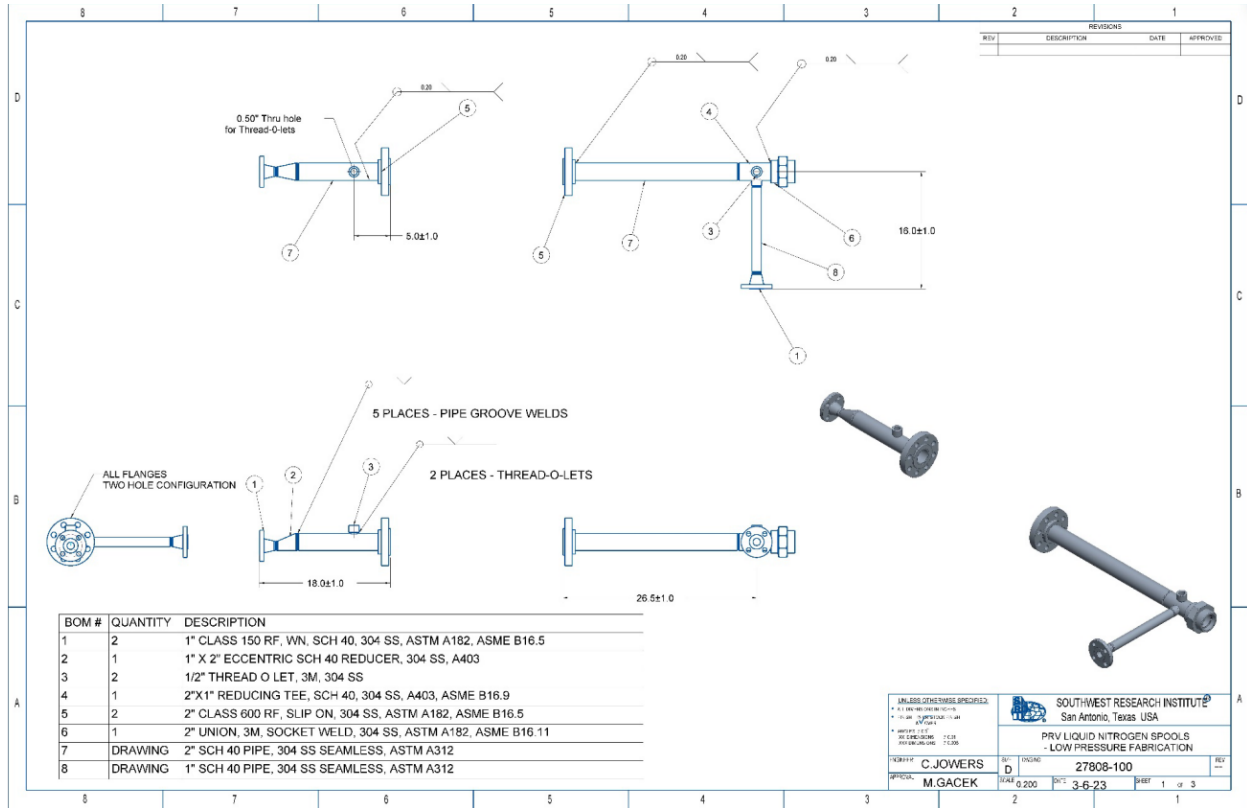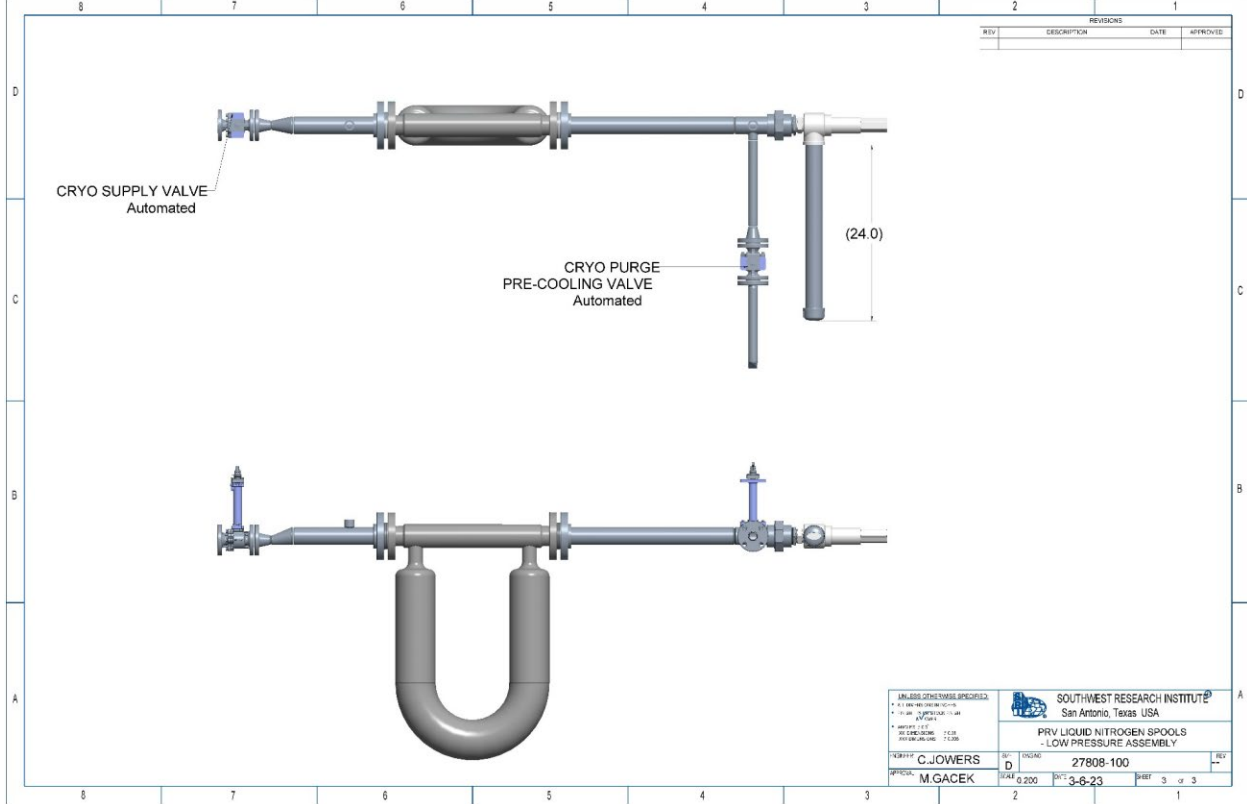# Appendix A

PRV Test System Setup

Appendix B

Test Section Fabrication and Setup Drawings

VB-27808-02

VB-27808-03

TEST PRV

SOUTHWEST RESEARCH INSTITUTE
San Antonio, Texas USA

PRV LIQUID NITROGEN SPOOLS
- LOW PRESSURE ASSEMBLY

C.JOWERS
M.GACEK
D   27808-100
SCALE 0.250   3-6-23   SHEET 2 OF 3

CRYO SUPPLY VALVE
Automated

CRYO PURGE
PRE-COOLING VALVE
Automated

(24.0)

SOUTHWEST RESEARCH INSTITUTE
San Antonio, Texas USA

PRV LIQUID NITROGEN SPOOLS
- LOW PRESSURE ASSEMBLY

C.JOWERS
M.GACEK
D   27808-100
SCALE 0.200   3-6-23   SHEET 3 OF 3

58

Abbreviations and Acronyms

ACRONYM	DEFINITION
ASME	American Society of Mechanical Engineers
BLEVE	Boiling Liquid Expanding Vapor Explosion
FDS	Fire Dynamics Simulator
FE	Finite Element
FRA	Federal Railroad Administration
HF	Heat Flux
HRR	Heat Release Rate
HRRPUA	Heat Release Rate Per Unit Area
ISO	International Organization for Standardization
LN2	Liquefied Nitrogen
LNG	Liquefied Natural Gas
MAWP	maximum allowable working pressure
NIST	National Institute of Standards and Technology
P&ID	piping and instrumentation diagram
PHMSA	Pipeline and Hazardous Materials Safety Administration
PPE	Personal Protective Equipment
PRV	Pressure Relief Valve
PTFE	Polytetrafluoroethylene
SCMS	Standard Cubic Meter Per Second
SwRI	Southwest Research Institute
TC	Thermocouple